Stereoelectronic Effects of the Arenophile (η^5-Cp*)Ru^+ in Electron-Rich σ-Arylacetylide Iron Complexes Including Redox-Driven Haptotropic Rearrangement: An Approach toward Readable Binary Molecular Memory Components

Jennifer A. Shaw-Taberlet,[†] Sourisak Sinbandhit,[‡] Thierry Roisnel,[†] Jean-René Hamon,*[,†] and Claude Lapinte*[,†]

UMR 6226 Sciences Chimiques de Rennes, CNRS−Université de Rennes 1, Campus de Beaulieu, 35042 Rennes Cedex, France, and Centre Régional de Mesures Physiques de l'Ouest, Université de Rennes 1, Campus de Beaulieu, 35042 Rennes Cedex, France

Received June 29, 2006

The organoiron vinylidene derivatives [(η^2-dppe)(η^5-Cp*)Fe═C═CH−(1-naphthyl)][X] (Cp* = C_5Me_5; dppe = 1,2-bis(diphenylphosphino)ethane; X = BPh_4, **3[BPh$_4$]**; X = PF_6, **3[PF$_6$]**) were synthesized from (η^2-dppe)(η^5-Cp*)FeCl and 1-naphthyl acetylene in the presence of $NaBPh_4$ or $NaPF_6$, respectively. The daughter organometallic acetylide complex, (η^2-dppe)(η^5-Cp*)Fe−C≡C−(1-naphthyl), **4**, was obtained, in 81% yield, upon deprotonation of the vinylidene precursor, **3[BPh$_4$]**, by *t*-BuOK in a MeOH/THF mixture at room temperature. One new dicationic heterobimetallic vinylidene Fe(II)−Ru(II) complex, **5[PF$_6$]$_2$**, was obtained, in 74% yield, upon reaction of the 1-naphthyl vinylidene precursor **3[PF$_6$]**, with [(η^5-Cp*)Ru($CH_3CN)_3$][PF_6]. Binuclear acetylides were prepared via η^6 complexation of the (η^5-Cp*)-Ru^+ arenophile onto either the substituted or the free naphthyl ring of 1-naphthyl acetylide derivative **4**, and both of these haptotropomers, **6A[PF$_6$]** and **6B[PF$_6$]**, were isolated. A third bimetallic model compound, **2[PF$_6$]**, was prepared in 69% yield via (η^5-Cp*Ru) coordination of the ethynyl phenyl ring of the known complex (η^2-dppe)(η^5-Cp*)Fe−C≡C−Ph (**1**). All three complexations are regioselective, occurring only on the acetylenic aryl moiety instead of the competing dppe phenyls. The thermally stable Fe^{III} counterparts, **2[PF$_6$]$_2$**, **4[PF$_6$]**, and **6B[PF$_6$]$_2$**, were obtained (70−86% isolated yield) upon oxidation, in THF at −60 °C, with ferrocenium hexafluorophosphate. All the new compounds were thoroughly authenticated using analytical and spectroscopic methods. In the heterobimetallic species, the aromaticity of the acetylide aryl linker is changed in situ via (i) the complexation of the (η^5-Cp*)Ru^+ arenophile and (ii) for the case of the 1-naphthyl substituent, by the $\eta^6-\eta^6$ inter-ring haptotropic migration of this group between naphthyl rings. The upshot is that these compounds exhibit significantly different degrees of electronic communication between the two organometallic termini across the length of the ethynediyl−aryl segment as a function of arenophile location: either (i) collinear to the Fe−C≡C wire-like segment (**2[PF$_6$]** and **6A[PF$_6$]**) or (ii) on the free ring of the 1-naphthyl moiety (**6B[PF$_6$]**). To establish the degree of electron transfer within the novel compounds reported herein, their physical properties are compared using NMR, UV-vis, IR, Mössbauer, and electron spin resonance (ESR) spectroscopies, as well as cyclic voltammetry and X-ray crystallography. Accordingly, the solid-state structures of all seven novel, electron-rich organometallic acetylides are described, including both haptotropomers **6A[PF$_6$]** and **6B[PF$_6$]**. Finally, the first redox-driven inter-ring haptotropic rearrangement of (η^5-Cp*)Ru^+ between naphthyl rings was shown to occur.

Introduction

The vast potential for the future use of molecules as building blocks of nanoscaled devices has inspired chemists to design and characterize compounds capable of performing useful functions within an as-yet hypothetical nanodevice. Specifically, in the fields of molecular and nanoelectronics,[1] nanodevices such as molecular wires[2] and switches[3] are described and occasionally attributed with information storage and processing potentials.[4] While the characterization of nanodevices remains a difficult problem, whether it takes place upon a single molecule within a nanoconnect or via the indirect methods employed here and elsewhere, electronic properties[5] of nanodevices are being increasingly published and compared. In order for a molecule to serve as a unit of binary computational memory, it must undergo a fast, solid-state transformation between two distinct states that are macroscopically distinguishable. Such a transformation could be made electronically, magnetically, or optically; however, a solution-state, chemical transformation would be poorly suited to application within a nanodevice. Finally,

* To whom correspondence should be addressed. E-mail: jean-rene.hamon@univ-rennes1.fr. Fax: +33 2 23 23 56 37. E-mail: claude.lapinte@univ-rennes1.fr. Fax: +33 2 23 23 59 63.

[†] UMR 6226.

[‡] CRMPO.

(1) (a) Robertson, N.; Mc. Gowan, G. A. *Chem. Soc. Rev.* **2003**, *32*, 96−103. (b) Caroll, R. L.; Gorman, C. B. *Angew. Chem., Int. Ed.* **2002**, *41*, 4379−4400. (c) Tour, J. M. *Acc. Chem. Res.* **2000**, *33*, 791−803. (d) Paul, F.; Lapinte, C. *Coord. Chem. Rev.* **1998**, *178*/*180*, 427−505. (e) Paul, F.; Lapinte, C. In *Unusual Structures and Physical Properties in Organometallic Chemistry*; Gielen, M., Willem, R., Wrackmeyer, B., Eds.; Wiley: San Francisco, 2002; pp 219−295.

10.1021/om060575q CCC: $33.50
Publication on Web 09/21/2006

distinctions between binary states should arise from spectroscopic or electronic data.

Inter-ring haptotropic rearrangement in which a metal migrates along a polyaromatic system has culminated in the design of organometallic switches. For instance, a recent study by Dötz and co-workers reported that the $\eta^6-\eta^6$ solution-state inter-ring haptotropic rearrangement of the $Cr(CO)_3$ arenophile on substituted naphthyl ligands proceeds photochemically in one direction and thermally in the other.[6] Other examples of irreversible[7] and chemically reversible switches[8] using solution-state haptotropic rearrangement of $Cr(CO)_3$ have also been reported. In addition, Benn and co-workers reported on the *intra-ring* haptotropic rearrangements of nickel complexes of naphthalene, which occur spontaneously in the solid state, as observed by NMR.[9]

In both theoretical[10] and experimental[11] discoveries published within recent years, mononuclear organoiron complexes in which a [(η^2-dppe)(η^5-Cp*)Fe] (dppe = 1,2-bis(diphenylphosphino)ethane; Cp* = C_5Me_5) redox-active terminus is σ-bonded to a *para*-substituted phenylethynyl spacer have served particularly well as molecular wire models (Scheme 1). For similar complexes, electron transfer and exchange processes have been determined to depend on the aromaticity of the conducting ligand.[12] In simple terms, the less aromatic the ligand, the more conductive the segment. To explain this empirical discovery, a resonance argument, summarized in Scheme 1, has been employed. Upon oxidation to Fe(III), a quinoidal, cumulenic mesomer IV contributes a 19-electron Fe(I). However, this structure perturbs the aromatic stabilization present in the aryl moiety. In conclusion, complexes containing fewer aromatic ligands, by favoring the quinoidal form, II and IV, exhibit better electronic transfer and exchange between termini.

Scheme 1. Definition of Type I Compounds and Selected Resonance Forms for Fe(II) and Fe(III) Species

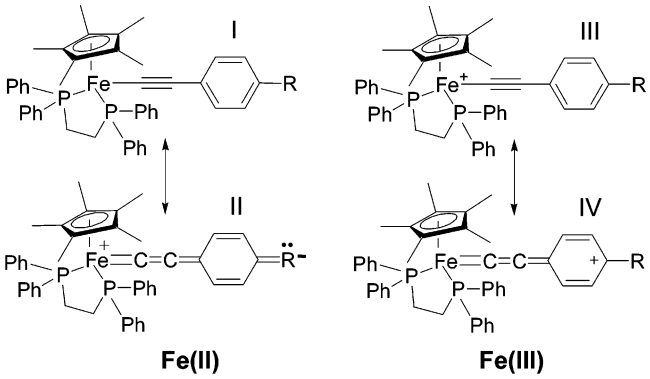

In the current study, we document the novel syntheses of the series of compounds shown in Scheme 2. Furthermore, we compare their differing capacities to conduct an electron across the length of the iron−ethynyl−aryl segment using multinuclear NMR, UV-vis, IR, Mössbauer, and electron spin resonance (ESR) spectroscopies, as well as cyclic voltammetry and X-ray crystallography. In addition, we endeavored to vary the aromaticity of the ligand in situ via the η^6 complexation of the 12-electron (η^5-Cp*)Ru^+ arenophile.[13] The Ru precursor was [(η^5-Cp*)Ru($CH_3CN)_3$][PF_6],[14] and complexation took place onto either naphthyl ring **A** (for complexation onto the acetylide, **4**) or ring **B** (for coordination onto the vinylidene, **3[PF$_6$]**, followed by reversible deprotonation), thus yielding both regioisomers of interest, **6A[PF$_6$]** and **6B[PF$_6$]** (Scheme 3). The difference in electron transfer properties between the resulting heterobinuclear species is macroscopically readable and identifies the binary states, **A** and **B**. Unfortunately, it was not possible to isolate more than a few crystals of haptotropomer **6A[PF$_6$]** in pure form (see Experimental Section). Therefore, the completely characterized model compound **2[PF$_6$]** is often compared to **6B[PF$_6$]** in place of **6A[PF$_6$]** in this proof of concept. Finally, chemically and redox-induced haptotropic rearrangements of the (η^5-Cp*)Ru^+ arenophile were shown to

(2) For studies in carbon-rich *organometallic* wires, see: (a) Rigaut, S.; Touchard, D.; Dixneuf, P. H. *Coord. Chem. Rev.* **2004**, *248*, 1585−1601. (b) Bruce, M. I.; Low, P. J. *Adv. Organomet. Chem.* **2004**, *50*, 179−444. (c) Szafert, S.; Gladysz, J. A. *Chem. Rev.* **2003**, *103*, 4175−4205. (d) Yam, V. W.-W. *Acc. Chem. Res.* **2002**, *35*, 555−563. (e) Powell, C. E.; Humphrey, M. G. *Coord. Chem. Rev.* **2004**, *248*, 725−756. For a recent review on *organic* molecular wires, see: (f) James, D. K.; Tour, J. M. *Top. Curr. Chem.* **2005**, *257*, 33−62.

(3) For some recent reviews, see: (a) Moussa, N. O.; Molnar, G.; Bonhommeau, S.; Zwick, A.; Mouri, S.; Tanaka, K.; Real, J. A.; Bousseksou, A. *Phys. Rev. Lett.* **2005**, *94*, 107205−107209. (b) Mendes, P. M.; Flood, A. H.; Stoddart, J. F. *Appl. Phys. A: Mater. Sci. Process.* **2005**, *80*, 1197−1209. (c) Benniston, A. C. *Chem. Soc. Rev.* **2004**, *33*, 573−578. (d) Bousseksou, A.; Molnar, G.; Matouzenko, G. *Eur. J. Inorg. Chem.* **2004**, 4353−4369.

(4) See for instance: (a) Cifuentes, M. P.; Humphrey, M. G.; Morall, J. P.; Samoc, M.; Paul, F.; Roisnel, T.; Lapinte, C. *Organometallics* **2005**, *24*, 4280−4288. (b) Hu, Q. Y.; Lu, W. X.; Tang, H. D.; Sung, H. H. Y.; Wen, T. B.; Williams, I. D.; Wong, G. K. L.; Lin, Z.; Jia, G. *Organometallics* **2005**, *24*, 3966−3973. (c) Fillaut, J.-L.; Perruchon, J.; Blanchard, P.; Roncali, J.; Gohlen, S.; Allain, M.; Migalska-Zalas, A.; Kityk, I. V.; Sahraoui, B. *Organometallics* **2005**, *24*, 687−695. (d) Venkatesan, K.; Blacque, O.; Fox, T.; Alfonso, M.; Schmalle, H. W.; Berke, H. *Organometallics* **2004**, *23*, 1183−1186. (e) Jiao, J.; Long, G. J.; Grandjean, F.; Beatty, A. M.; Fehlner, T. P. *J. Am. Chem. Soc.* **2003**, *125*, 7522−7523. (f) Wong, K. M.-C.; Lam, S. C.-F.; Ko, C.-C.; Zhu, N.; Yam, V. W.-W.; Roue, S.; Lapinte, C.; Fathallah, S.; Costuas, K.; Kahlal, S.; Halet, J.-F. *Inorg. Chem.* **2003**, *42*, 7086−7097. (g) Powell, C. E.; Humphrey, M. G.; Cifuentes, M. P.; Morall, J. P.; Samoc, M.; Luther-Davies, B. *J. Phys. Chem. A* **2003**, *107*, 11264−11266. (h) Naklicki, M. L.; White, C. A.; Plante, L. L.; Evans, C. E. B.; Crutchley, R. J. *Inorg. Chem.* **1998**, *37*, 1880−1885.

(5) For one recent review of direct conduction measurements, see: (a) James, D. K.; Tour, J. M. *Chem. Mater.* **2004**, *16*, 4423−4435. For electron transfer studies, see: (b) Benniston, A. C.; Harriman, A. *Chem. Soc. Rev.* **2006**, *35*, 169−179. (c) Ren, T. *Organometallics* **2005**, *24*, 4854−4870. (d) Crutchley, R. J. *Adv. Inorg. Chem.* **1994**, *41*, 273−325. (e) Schwab, P. F. H.; Levin, M. D.; Michl, J. *Chem. Rev.* **1999**, *99*, 1863−1933. (f) Schwab, P. F. H.; Smith, J. R.; Michl, J. *Chem. Rev.* **2005**, *105*, 1197−1279. (g) Qi, H.; Gupta, A.; Noll, B. C.; Snider, G. L.; Lu, Y.; Lent, S. S.; Fehlner, T. P. *J. Am. Chem. Soc.* **2005**, *127*, 15218−15227. (h) Blum, A. S.; Ren, T.; Parish, D. A.; Trammell, S. A.; Moore, M. H.; Kushmerick, J. G.; Xu, G.-L.; Deschamps, J. R.; Polack, S. K.; Shashidar, R. *J. Am. Chem. Soc.* **2005**, *127*, 10010−10011. (i) Xu, G.-L.; Crutchley, R. J.; DeRosa, M. C.; Pan, Q.-J.; Zhang, H.-X.; Wang, X.; Ren, T. *J. Am. Chem. Soc.* **2005**, *127*, 13354−13365. (j) Schull, T. L.; Kushmerick, J. G.; Patterson, C. H.; George, C.; Moore, M. H.; Pollack, S. K.; Shashidhar, R. *J. Am. Chem. Soc.* **2003**, *125*, 3202−3203. (k) Astruc, D. *Electron Transfer and Radical Processes in Transition-Metal Chemistry*; VCH: New York, 1995.

(6) (a) Jahr, H. C.; Nieger, M.; Dötz, K. H. *Chem. Commun.* **2003**, 2866−2867. (b) Dötz, K. H.; Jahr, H. C. *Chem. Rec.* **2004**, *4*, 61−71. (c) Jahr, H. C.; Nieger, M.; Dötz, K. H. *Chem. Eur. J.* **2005**, *11*, 5333−5342. (d) Dötz, K. H.; Wenzel, B.; Jahr, H. C. *Top. Curr. Chem.* **2004**, *248*, 63−103.

(7) (a) Pan, J.; Wang, J.; Nanaszak, M. M.; Kampf, J. W.; Ashe, A. J., III. *Organometallics* **2006**, *25*, 3463−3467, see also references therein. (b) Oprunenko, Y. F. *Russ. Chem. Rev.* **2000**, *69*, 683−704.

(8) Pan, J.; Kampf, J. W.; Ashe, A. J., III. *Organometallics* **2006**, *25*, 197−202.

(9) Benn, R.; Mynott, R.; Topalovic, I.; Scott, F. O*rganometallics* **1989**, *8*, 2299−2305.

(10) Costuas, K.; Paul, F.; Toupet, L.; Halet, J.-F.; Lapinte, C. *Organometallics* **2004**, *23*, 2053−2068.

(11) (a) Denis, R.; Toupet, L.; Paul, F.; Lapinte, C. *Organometallics* **2000**, *19*, 4240−4251. (b) Paul, F.; Mevellec, J.-Y.; Lapinte, C. *Dalton Trans.* **2002**, 1783−1790. (c) Paul, F.; Toupet, L.; Thepot, J.-Y.; Costuas, K.; Halet, J.-F.; Lapinte, C. *Organometallics* **2005**, *24*, 5464−5478.

(12) (a) de Montigny, F.; Argouarch, G.; Costuas, K.; Halet, J.-F.; Roisnel, T.; Toupet, L.; Lapinte, C. *Organometallics* **2005**, *24*, 4558−4572. (b) Ibn-Ghazala, S.; Paul, F.; Toupet, L.; Roisnel, T.; Hapiot, P.; Lapinte, C. *J. Am. Chem. Soc.* **2006**, *128*, 2463−2476. (c) Shaw-Taberlet, J. A.; Hamon, J.-R.; Lapinte, C. Unpublished work.

(13) Fagan, P. J.; Ward, M. D.; Calabrese, J. C. *J. Am. Chem. Soc.* **1989**, *111*, 1698−1719.

(14) Mbaye, M. D.; Demerseman, B.; Renaud, J.-L.; Toupet, L.; Bruneau, C. *Adv. Synth. Catal.* **2004**, *346*, 835−841.

Scheme 2. Novel Iron Ethynyl and Vinylidene Complexes Described Herein

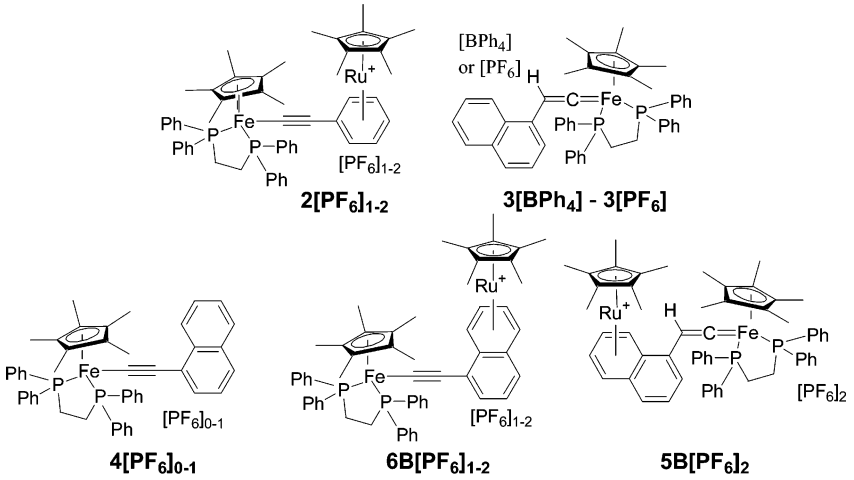

Scheme 3. Definitions of Regioisomers A and B

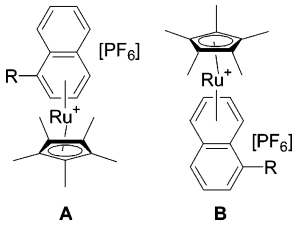

occur at room temperature to a limited extent between the two naphthyl rings upon in situ variation of the electronic and steric environment.

Results and Discussion

Syntheses of the Mononuclear Iron(II) Complexes. To obtain the novel organoiron vinylidenes, **3[BPh4]** and **3[PF6]**, 1-naphthyl acetylene was reacted, in a methanol/THF mixture, with (η^2-dppe)(η^5-Cp*)FeCl in the presence of either $NaBPh_4$ or $NaPF_6$, as shown in Scheme 4. Both vinylidene syntheses are comparable in terms of yield and facility of purification. The two salts were isolated in 94 and 83% yield, respectively, as brown solids. These are stable for long periods at room temperature under argon, and dry samples display air-stability for short periods.

The daughter acetylide complex, (η^2-dppe)(η^5-Cp*)Fe−C≡C−(1-naphthyl), **4**, was obtained upon deprotonation of the vinylidene precursor, **3[BPh4]**, by an excess (1.2 equiv) of potassium *tert*-butoxide in a MeOH/THF mixture at room temperature. Complex **4** was isolated in 81% yield as an air- and moisture-sensitive orange powder. This derivative can also be prepared (70% overall yield) via the one-pot route in which the two steps shown in Scheme 4 are combined.

Syntheses of the Heterobinuclear Fe(II)/Ru(II) Complexes. In general, the heterobimetallic complexes were obtained upon η^6 complexation of the arylvinylidene or arylethynyl iron(II) by [(η^5-Cp*)Ru(CH_3CN)$_3$][PF_6]. For example, novel binuclear complex **2[PF6]** was prepared in 69% yield and isolated as a red powder, from the known ethynylphenyl derivative (η^2-dppe)-(η^5-Cp*)Fe−C≡C−Ph, **1**,[11,15] as shown in Scheme 5. Given stoichiometric conditions, this reaction is regioselective; complexation occurs only on the acetylenic phenyl moiety, never on the competing dppe phenyls.

The yellow heterobinuclear vinylidene 1-naphthyl derivative **5B[PF6]2** was synthesized in 74% isolated yield, via an analogous procedure (Scheme 6). ^{1}H NMR showed that the crude mixture included regioisomers **A** and **B** (Scheme 3). However, the small yield (8%) of isomer **A** was easily removed along with excess starting material by partial precipitation of a dichloromethane solution of the mixture in pentane followed by multiple washings with a 50:1 mixture of THF and dichloromethane until the rinses were colorless. Once again, side-complexation onto dppe phenyls was ruled out by careful characterization (see Experimental Section). The daughter bimetallic acetylides, **6A[PF6]** and **6B[PF6]**, were made via two routes, the former giving rise to a mixture of isomers **A** and **B**, and the latter affording only regioisomer **B**. These two *modus operandi* are shown in Scheme 6. The first procedure yields a 47:53 ratio of regioisomers **6A[PF6]**:**6B[PF6]**, determined by ^{1}H NMR spectroscopy before purification. Due to the differing solubilities of the isomers, partial precipitation, a common method of purification, artificially changes this fraction. Thus, a few orange crystals of **6A[PF6]** were isolated after slow diffusion of pentane into a THF solution of the mixture of regioisomers. In contrast, analytically pure isomer **6B[PF6]** was prepared as a very dark powder in 80% isolated yield upon deprotonation of the dicationic bimetallic vinylidene derivative **5B[PF6]2** with 1.3 equiv of *t*-BuOK, in methanol at room temperature for 2 h. Dry samples of the above-described heterobimetallic species **6A[PF6]** and **6B[PF6]** display good thermal stability in air.

In agreement with the two previous reactions (syntheses of **2[PF6]** and **5B[PF6]2**), the complexations in Scheme 6 never involve the dppe phenyls unless an excess of the ruthenium precursor is used. Given the body of work relating the consistent preference of arenophiles for phenyl rings versus naphthyl ones, this result is certainly interesting. For example, in a seminal study, Nolan, Fagan, and co-workers established the enthalpies of the complexations of (η^5-Cp*)Ru^+ onto naphthalene and various substituted benzenes and found that the naphthalene complex was formed the least favorably ($\Delta H = -1.7$ kcal/mol) and that complexation onto substituted benzenes became more and more favorable the more electron-donating the substituents.[16] Furthermore, Fagan et al.[13] reported the facile complexation of the (η^5-Cp*)Ru^+ arenophile onto all four phenyl rings of tetraphenyl methane. Given the fact that the tetrahedral dppe site provides an analogous steric and electronic environment, it

(15) Connelly, N. G.; Gamasa, M. P.; Gimeno, J.; Lapinte, C.; Lastra, E.; Maher, J. P.; Le Narvor, N.; Rieger, A. L.; Rieger, P. H. *J. Chem. Soc., Dalton Trans.* **1993**, 2575−2578.

(16) Nolan, S. P.; Martin, K. L.; Stevens, E. D.; Fagan, P. J. *Organometallics* **1992**, *11*, 3947−3953.

Scheme 4. Syntheses of the Vinylidenes, 3[BPh_4] and 3[PF_6], and the Corresponding Acetylide 4[a]

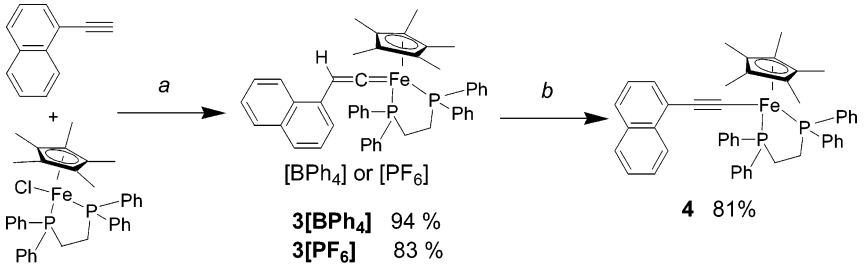

[a] Key reagents: (a) $NaBPh_4$ or $NaPF_6$, 20 °C, MeOH/THF, 16 h; (b) $KBuO^t$, 20 °C, MeOH, THF, 2 h.

Scheme 5. Regioselective Synthesis of 2[PF_6]

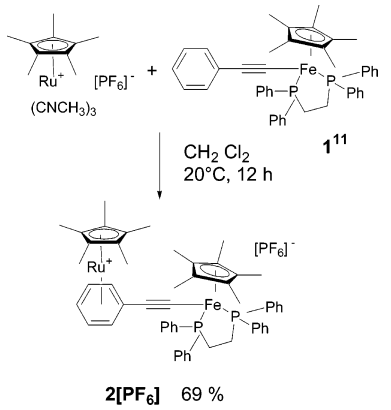

Scheme 6. Synthesis of 6A[PF_6] (top) and Regioselective Synthesis of 6B[PF_6] (bottom)

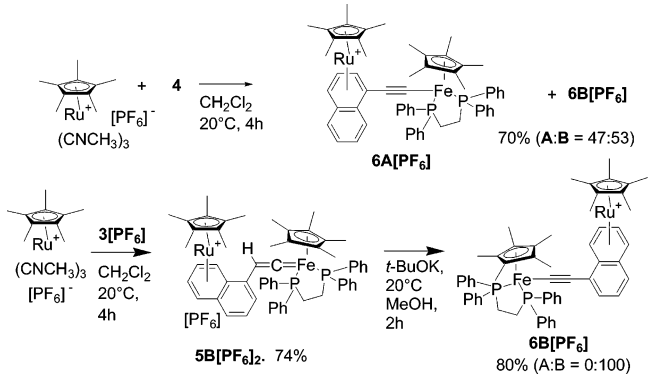

is quite surprising, but interesting, that our reactions are regiospecific in preference of the naphthalene. Another example of arenophile preference for a fused ring moiety in the presence of phenyl groups has previously been reported for [(η^5-Cp*)Ru(η^6-rubrene)][O_3SCF_3] (rubrene = 5,6,11,12-tetraphenylnaphthacene).[17] In this work, the (η^5-Cp*)Ru^+ unit was bound to the outermost ring of the naphthacene functionality under certain conditions.

Interestingly, preliminary results show that complexation by the arenophile (η^5-Cp*)Ru^+ onto the dppe phenyls of (η^2-dppe)(η^5-Cp*)Fe−R *does* occur in some cases. Two such cases were observed within our group and will be published in detail in a following paper.[12c] The first such dppe phenyl complexation took place on a common precursor, (η^2-dppe)(η^5-Cp*)FeCl, a compound in which no other aromatic rings were available. Another was observed in bimetallic species when all other aromatic rings were quite sterically encumbered, and the dppe groups were attached to very electron-rich sites linked by a 1,4-bisethynylaryl spacer.

(17) Fagan, P. J.; Ward, M. D.; Calabrese, J. C.; Caspar, J. V.; Krusic, P. J. *J. Am. Chem. Soc.* **1988**, *110*, 2981−2983.

Scheme 7. Syntheses of the Mono- and Binuclear Fe(III) and Fe(III)−Ru(II) Complexes[a]

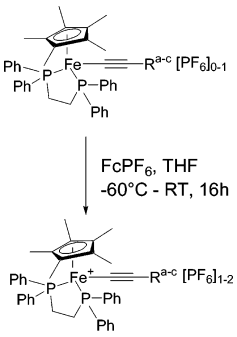

(a) R = (η^5-C_5Me_5)Ru[η^6-(phenyl)]; (b) R = 1-naphthyl; (c) R = (η^5-C_5Me_5)Ru[η^6-(naphthyl)].

Syntheses of the Mono- and Binuclear Fe(III) and Fe(III)−Ru(II) Complexes. Chemical oxidation, in THF at −60 °C, of the iron(II) products **2[PF_6]**, **4**, and **6B[PF_6]** gave the corresponding, thermally stable paramagnetic iron(III) counterparts, **2[PF_6]$_2$**, **4[PF_6]**, and **6B[PF_6]$_2$**, respectively, in the presence of ferrocenium hexafluorophosphate (Scheme 7). In all cases, good to high yields (70−86%) were consistently obtained, and purification by partial precipitation using common organic solvents provided spectroscopically pure material (see Experimental Section).

All of these new complexes were structurally characterized by the usual spectroscopies (FT-IR, UV−vis, ^{1}H, ^{13}C, and ^{31}P NMR), ESI high-resolution mass spectrometry, and cyclic voltammetry. Furthermore, the crystal structures of all of the organometallic acetylide complexes were resolved. While satisfactory elemental analyses were obtained in most cases, all compounds were found to be spectroscopically pure. Moreover, the paramagnetic iron(III) derivatives were characterized by electron spin resonance (ESR) and Mössbauer spectrometry.

NMR Spectroscopy. The relevant ^{1}H, ^{13}C, and ^{31}P NMR data of the mononuclear complexes agree well with those of previously described, related compounds in the (η^2-dppe)(η^5-Cp*)Fe series.[11,18] Thus, the vinylidene precursors **3[BPh_4]** and **3[PF_6]** exhibited the characteristic features of the iron−vinylidene core, Fe═C_α═C_βH−, with the triplets assigned to the vinylidene protons at δ = 5.79 and 5.76 ppm, respectively, with a coupling constant $^4J_{H-P}$ = 4.0 Hz, in their ^{1}H NMR spectra, and the downfield triplet resonance of the C_α nucleus at 356.7 ppm with a $^2J_{C-P}$ of 33 Hz in the ^{13}C NMR spectrum of **3[BPh_4]**. In addition, the NMR spectra of 18- and 17-electron ethynyl-1-naphthyl iron molecules, **4** and **4[PF_6]** (the latter being paramagnetic, no ^{13}C spectrum is reported herein), *very* closely resemble those of related compounds **1** and **1[PF_6]**, as expected.[11,15] In the ^{31}P NMR spectrum of **4**, the single signal observed at 101.0 ppm is characteristic of an acetylide iron(II)

complex, and the ^{13}C NMR spectrum shows the triplet ($^2J_{C-P}$ = 39.2 Hz) and singlet signatures for the acetylide linkage at δ = 145.1 and 119.7 ppm, respectively. The ^{31}P NMR signal of the dppe groups of paramagnetic **4[PF$_6$]** was possibly found at 315 ppm (br s, $w_{1/2}$ = 21 200 Hz), making this one of the rare iron(III) compounds studied in our laboratory for which the dppe signal was observed.[19]

Upon complexation to (η^5-Cp*)Ru$^+$, ^1H and ^{13}C chemical shifts attributed to the complexed aromatic ring of **2[PF$_6$]**, **6A-[PF$_6$],** and **6B[PF$_6$]** undergo an upfield shift, as usual for η^6-arene metal complexes.[20] In addition, the arenophile of these four compounds is observed via the presence of one and two sharp singlets in the ^1H and $^{13}C\{^1H\}$ NMR spectra, respectively (see Experimental Section). The two regioisomers **6A[PF$_6$]** and **6B[PF$_6$]** are easily distinguishable using room-temperature ^1H NMR by their resolved upfield signals ($6.54 < \delta < 5.58$ and $6.55 < \delta < 6.08$) of cumulative relative intensities 3H and 4H that correspond to the complexed ring protons. Furthermore, the dppe phosphorus nuclei are split as in an AB system in the ^{31}P NMR spectra of **5B[PF$_6$]$_2$**, **6A[PF$_6$]**, and **6B[PF$_6$]**, whereas the corresponding organoiron precursors, **3[PF$_6$]** and **4**, are each characterized by a singlet (see above). The AB system doublet is further split into a smaller doublet, because the heterobinuclear species are planar chiral. Therefore, the enantiotopic phosphorus atom of each enantiomer within the racemic mixtures is distinguishable by between 15 and 30 Hz.

The bulky arenophile also introduces coalescence into the spectra, giving rise to the temperature dependence of certain peaks in the ^1H and ^{31}P spectra and resulting in the decreasing of the intensity and broadening of dppe signals (both in ^1H and ^{31}P spectra) and (η^5-Cp*)Fe signals (both in ^1H and ^{13}C spectra). This coalescence is surely due to steric strain, observed in the crystal structures of all novel heterobinuclear species described herein (vide infra). It is noteworthy that both NMR and X-ray crystallography show a larger degree of strain between the dppe ligand and (η^5-Cp*)Ru$^+$ group for compound **6A[PF$_6$]**, whereas strain between the two Cp* entities is greater for compound **6B[PF$_6$]**.

Variable-temperature NMR spectra were taken of crystals of both **6A[PF$_6$]** and **6B[PF$_6$]** dissolved in acetone-d_6 in attempts to observe the beginning and end of the coalescence phenomenon. For the first regioisomer, between 193 and 243 K, the ^{31}P spectrum showed no coalescence, and the signal is split into a sharp, well-defined doublet of doublets. With increasing temperature, the doublets converge and broaden and their intensities decrease. To explain the spectral data, we conclude that rotation about the carbon bridge between the two organometallic termini is sterically restricted by the bulky, terminal dppe and Cp* ligands. At low temperatures, well-resolved spectra of one rotamer is possible, but as the temperature rises, molecular motion creates a poorly defined average due to the restrained wagging of the terminal moieties. Heating up to 343 K in THF was not adequate to give rise to a different, spectrally unique, rotamer, and the spectra remained identical.

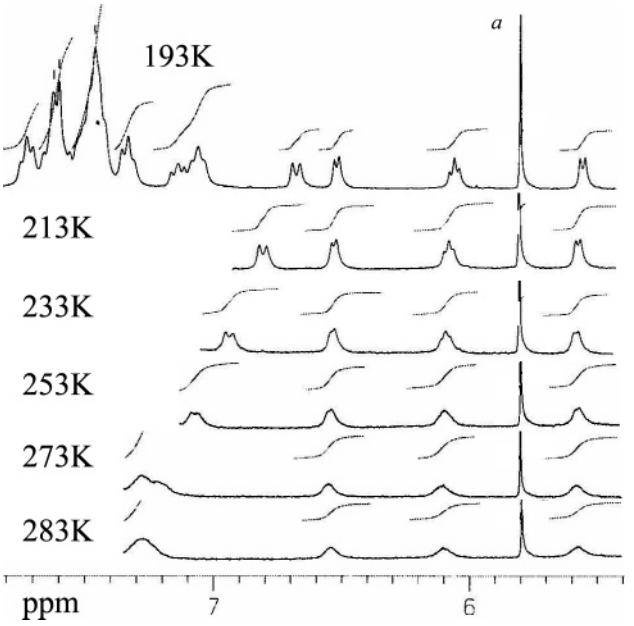

Figure 1. Aromatic region of the high-field ^1H NMR spectra (500 MHz) of **6A[PF$_6$]** at various temperatures in acetone-d_6. The singlet (*a*) is due to the crystallization solvent.

Table 1. IR νC≡C Bond Stretching[a]

compd	Fe(II)	Fe(III)	$\Delta\nu_{C\equiv C}$	ref
1[PF$_6$]$_n$	2053[b]	2021, 1988[c]	−32, −65	7a
2[PF$_6$]$_n$	2028, 1982[c]	2042[d]	+14, +60	this work
4[PF$_6$]$_n$	2040[b]	1988, 1918[c]	−62, −122	this work
6B[PF$_6$]$_n$	2026[c]	2026, 1978[d]	0, −22	this work

[a] In Nujol, cm^{-1}. [b] $n = 0$. [c] $n = 1$. [d] $n = 2$.

From variable-temperature ^1H NMR experiments of this same compound, **6A[PF$_6$]**, another very interesting observation arose (Figure 1). At low temperatures, the three shielded, aromatic protons of the complexed naphthyl ring, sounding off between 6.5 and 5.4 ppm, are joined by an additional doublet integrating at 2 protons. In contrast, all other noncomplexed aromatic signals remain at much lower field, between 8.1 and 7.0 ppm. As the temperature rises, this errant doublet, witness to a dynamic process, traverses the void between complexed and free aromatic regions of the spectrum. This signal can be attributed to two *ortho* protons of the dppe phenyl groups, due to their proximity to the ruthenium atom, as observed in the crystal structure (see Figure 2g).

As for the other regioisomer, while the aromatic signals in the ^1H spectrum do travel as a function of temperature, the signals attributed to the complexed ring in **6B[PF$_6$]** remain the

(18) (a) Roue, S.; Lapinte, C. *J. Organomet. Chem.* **2005**, *690*, 594−604. (b) Bruce, M. I.; Costuas, K.; Davin, T.; Ellis, B. G.; Halet, J.-F.; Lapinte, C.; Low, P. J.; Smith, M. E.; Skelton, B. W.; Toupet, L.; White, A. H. *Organometallics* **2005**, *24*, 3864−3881. (c) Paul, F.; Ellis, B. G.; Bruce, M. I.; Toupet, L.; Roisnel, T.; Costuas, K.; Halet, J.-F.; Lapinte, C. O*rganometallics* **2006**, *25*, 649−665. (d) Bruce, M. I.; Low, P. J.; Hartl, F.; Humphrey, P. A.; de Montigny, F.; Jevric, M.; Lapinte, C.; Perkins, G. J.; Roberts, R. L.; Skelton, B. W.; White, A. H. *Organometallics* **2005**, *24*, 5241−5255. (e) Bruce, M. I.; De Montigny, F.; Jevric, M.; Lapinte, C.; Skelton, B. W.; Smith, M. E.; White, A. H. *J. Organomet. Chem.* **2004**, *689*, 2860−2871. (f) Bruce, M. I.; Ellis, B. G.; Gaudio, M.; Lapinte, C.; Melino, G.; Paul, F.; Skelton, B. W.; Smith, M. E.; Toupet, L.; White, A. H. *Dalton Trans.* **2004**, 1601−1609. (g) Roue, S.; Lapinte, C.; Bataille, T. *Organometallics* **2004**, *23*, 2558−2567. (h) Costuas, K.; Paul, F.; Toupet, L.; Halet, J.-F.; Lapinte, C. *Organometallics* **2004**, *23*, 2053−2068. (i) Coat, F.; Paul, F.; Lapinte, C.; Toupet, L.; Costuas, K.; Halet, J.-F. *J. Organomet. Chem.* **2003**, *683*, 368−378. (j) Roue, S.; Le Stang, S.; Toupet, L.; Lapinte, C. *C. R. Chimie* **2003**, *6*, 353−366. (k) Jiao, H.; Costuas, K.; Gladysz, J. A.; Halet, J.-F.; Guillemot, M.; Toupet, L.; Paul, F.; Lapinte, C. *J. Am. Chem. Soc.* **2003**, *125*, 9511−9522. (l) Argouarch, G.; Thominot, P.; Paul, F.; Toupet, L.; Lapinte, C. *C. R. Chimie* **2003**, *6*, 209−222. (m) Courmarcel, J.; Le Gland, G.; Toupet, L.; Paul, F.; Lapinte, C. *J. Organomet. Chem.* **2003**, *670*, 108−122.

(19) (a) Guillaume, V.; Mahias, V.; Mari, A.; Lapinte, C. *Organometallics* **2000**, *19*, 1422−1426. (b) Fettinger, J. C.; Mattamana, S. P.; Poli, R.; Rogers, R. D. *Organometallics* **1996**, *15*, 4211−4222. (c) Weyland, T.; Costuas, K.; Mari, A.; Halet, J.-F.; Lapinte, C. *Organometallics* **1998**, *17*, 5569−5579.

(20) Hubig, S. M.; Lindeman, S. V.; Kochi, J. K. *Coord. Chem. Rev.* **2000**, *200−202*, 831−873.

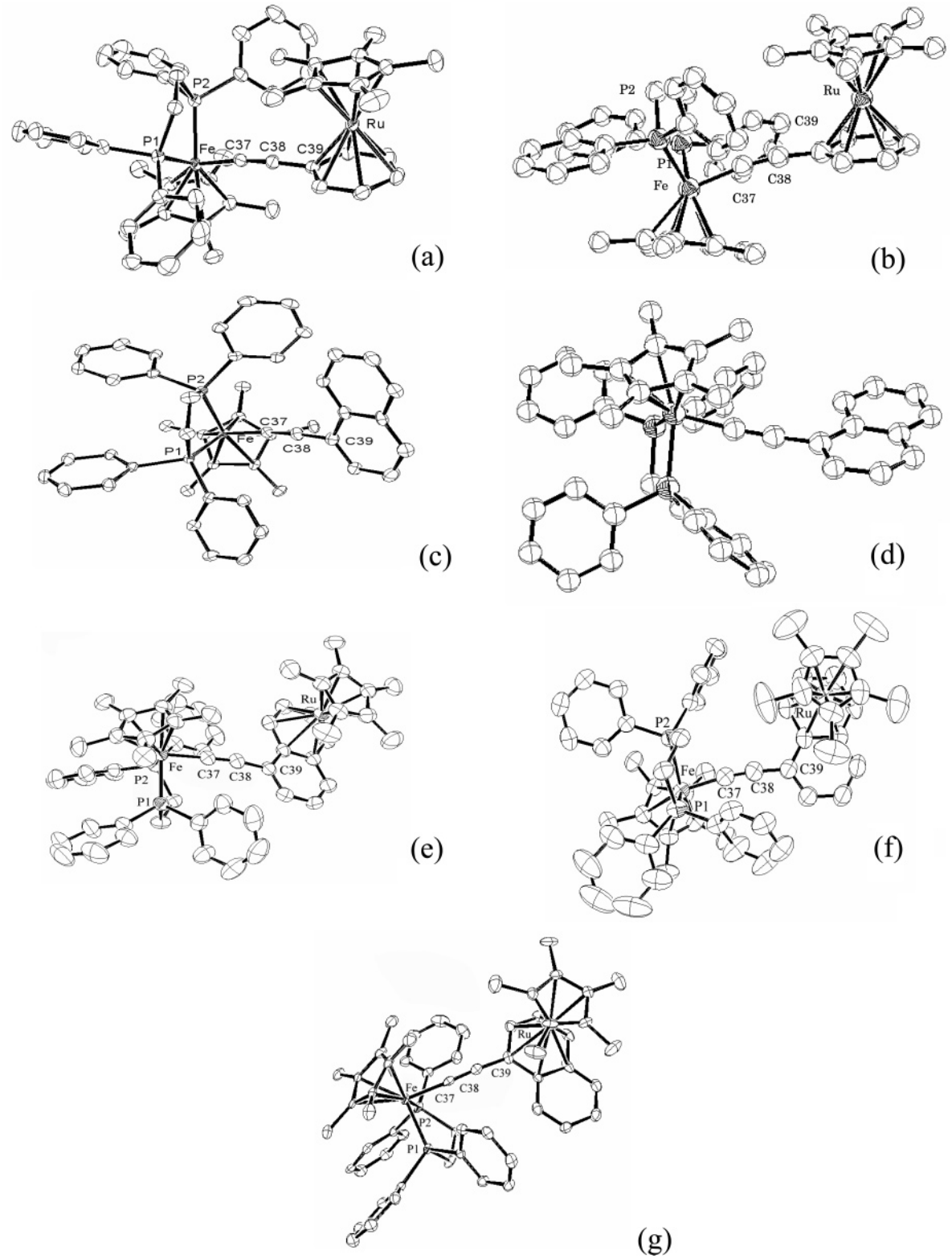

Figure 2. ORTEP diagram at 50% probability level for (a) **2[PF$_6$]**; (b) **2[PF$_6$]$_2$**; (c) **4**; (d) **4[PF$_6$]**; (e) **6B[PF$_6$]**; (f) **6B[PF$_6$]$_2$**; (g) **6A[PF$_6$]**.

only ones to appear between 5.7 and 6.7 ppm at all temperatures. In other words, the dppe phenyl rings seem to remain outside of the shielding cone of the ruthenium atom. In conclusion, rotation about the Fe−C37 and C38−C39 (see Figure 2 for the labeling scheme) bonds is hindered in **6A[PF$_6$]** and **6B[PF$_6$]**, probably due to steric constraints.

Infrared Spectroscopy. Table 1 reports IR absorption bands due to the C≡C stretching mode of the novel organometallic acetylides and the related **1[PF$_6$]$_n$** (n = 0, 1).[11a] For iron(II) cases in which a degree of contribution from mesomer II, shown in Scheme 1, becomes favored, a decrease in IR stretching frequency is expected. In other words, as the delocalization of electron density from iron to the carbon-rich ligand increases, the frequency of the IR stretch decreases, as has been reported.[11,15] Such delocalization in type I compounds, however, comes at a cost due to the loss in aromatic stabilization upon perturbation of the (4n+2) aromatic electron count. Therefore, it is not surprising that the IR stretch is lower for the naphthyl

Table 2. Crystal Data, Collection, and Refinement Parameters

	2[PF$_6$]	**2[PF$_6$]$_2$**	**4**	**4[PF$_6$]**	**6A[PF$_6$]**	**6B[PF$_6$]**	**6B[PF$_6$]$_2$**
formula	$C_{54}H_{59}F_6P_3FeRu\cdot CH_2Cl_2$	$3C_{54}H_{59}F_{12}FeP_4Ru\cdot 4CH_2Cl_2$	$C_{48}H_{46}P_2Fe$	$C_{48}H_{46}F_6P_3Fe$	$C_{58}H_{61}P_3FeF_6Ru\cdot CH_2Cl_2$	$C_{58}H_{61}P_3FeF_6Ru\cdot CH_2Cl_2$	$C_{58}H_{61}F_{12}FeP_4Ru\cdot CH_3CN$
fw	1142.74	5171.25	740.64	885.61	1206.82	1206.82	1307.92
temp (K)	293(2)	100(2)	100(2)	100(2)	293(2)	293(2)	293(2)
cryst syst	monoclinic	monoclinic	triclinic	monoclinic	triclinic	triclinic	monoclinic
space group	*C*2/*c*	$P2_1/n$	$P\bar{1}$	$P2_1/a$	$P\bar{1}$	$P\bar{1}$	$P2_1/c$
a (Å)	31.623(5)	31.5094(18)	8.5490(4)	12.1157(4)	13. 113(5)	12.611(5)	16.9349(4)
b (Å)	19.517(5)	12.6356(7)	11.9143(6)	30.6594(10)	16.069(5)	15.465(5)	14.5532(3)
c (Å)	20.576(5)	45.491(3)	19.4745(9)	12.1468(4)	16.817(5)	15.726(5)	22.8752(5)
α (deg)	90	90	91.627(2)	90	117.596(5)	73.519(5)	90
β (deg)	125.645(5)	92.890(3)	100.166(3)	107.230(2)	92.541(5)	79.923(5)	96.1740(10)
γ (deg)	90	90	103.780(2)	90	105.820(5)	72.445(5)	90
V (Å^3)	10320(4)	18089(2)	1891(0.2)	4310(0.2)	2960(2)	2791(2)	5605(0.2)
Z	8	12	2	4	2	2	4
D_{calc} (g cm^{-3})	1.471	1.341	1.301	1.365	1.282	1.436	1.55
cryst size (mm)	0.7 × 0.5 × 0.4	0.4 × 0.2 × 0.02	0.3 × 0.25 × 0.1	0.28 × 0.15 × 0.04	0.5 × 0.4 × 0.3	0.5 × 0.4 × 0.3	0.8 × 0.4 × 0.1
F(000)	4688	7452	780	1836	1170	1240	2676
abs coeff, μ (mm^{-1})	0.828	0.666	0.517	0.521	0.636	0.77	0.723
θ range (deg)	0.998−27.485	0.77−27.50	1.07−27.57	1.76−27.50	3.51−30.06	1.36−34.93	2.66−27.50
hkl range	−41 to +40, −25 to +25, −25 to +26	−40 to +40, −14 to +16, −58 to +58	−11 to +11, −15 to +15, −21 to +25	−14 to +15, −39 to +38, −15 to +15	−15 to +17, −22 to +22, −23 to +23	−19 to +20, −24 to +24, −24 to +24	−21 to +21, −18 to +17, −29 to +29
total no. of reflns	10 840	41 218	29 196	36 332	14 252	21 521	23 838
no. of unique reflns	6775	15 406	8489	9863	7898	14 935	12 819
no. of restrs/params	0/614	0/1885	0/461	0/532	0/703	0/649	0/714
a, *b* for *w*[a]	0.0305, 85.5961	0.0893, 0	0.0600, 0.7368	0.0661, 9.3346	0.0871, 8.6493	0.1151, 1.2884	0.0655, 10.4225
R_1	0.048	0.0884	0.0426	0.0708	0.0619	0.0565	0.0679
R_w	0.1034	0.2070	0.1062	0.1611	0.1508	0.1669	0.158
R_1 (all data)	0.1082	0.1985	0.0612	0.1261	0.1410	0.0845	0.1177
R_w (all data)	0.1454	0.2375	0.1201	0.1814	0.2097	0.1941	0.1832
goodness of fit/F^2	1.145	0.986	1.117	1.039	1.044	1.026	1.059
refine diff density max., min. (e Å^{-3})	1.182, −0.746	1.588, −1.774	1.015, −0.465	1.047, −0.629	0.953, −0.874	3.139, −0.734	0.702, −0.527

iron(II) derivative **4** than for the phenyl one **1**, because the naphthyl ring is less aromatic than the phenyl one.[21]

Alternately, a contribution from cumulenic mesomer IV (Scheme 1) can occur upon the oxidation of the iron atom, as electron density is transferred across the ethynyl linker toward the 17-electron iron. For example, the IR stretching frequency decreases for both the phenyl **1[PF$_6$]** and naphthyl **4[PF$_6$]** iron(III) acetylides versus their iron(II) precursors. The comparison between oxidation states enables us to report that the phenyl and naphthyl aromatic rings act as better electron donors than acceptors. Delocalization across the C≡C bond occurs more readily from the aromatic ring toward an electron-deficient iron than from an electron-rich iron toward the aromatic ring. Furthermore, the difference in frequency between the iron(II) and iron(III) species is larger for the naphthyl species, which is, once again, explained by its lower aromaticity relative to the phenyl product. The important conclusion to be drawn is that the significant reduction of the value of this IR stretch implies good conduction of electron density along the acetylene carbons. Despite the relative simplicity of these data, it should be remembered that the frequency of the stretching mode depends not only on the C≡C bond order but also on the masses of the termini.[22] This size effect also plays a role in stretching frequency reductions observed between **1** and **2[PF$_6$]** and between **4** and **6B[PF$_6$]**.

Interestingly, compounds **2[PF$_6$]** and **2[PF$_6$]$_2$** display a relationship opposite that previously observed among the plethora of known compounds of type I.[11a] These unique products result in IR stretching frequencies for the iron(III) compounds that are significantly *larger* than those for the corresponding iron(II) species, in agreement with the shortening of the C−C bond length of ca. 0.01 Å upon oxidation of **2-[PF$_6$]** to **2[PF$_6$]$_2$** (see Table 3). These data suggest that the contribution from cumulenic resonance structure II (Scheme 1) is larger in the iron(II) compound than in mesomer IV for the iron(III) derivative. This phenomenon can be rationalized using two arguments. First, the connection of the electron-rich iron(II) arylalkynyl moiety with (η^5-Cp*)Ru$^+$, a cationic electron-withdrawing group, naturally explains the importance of mesomer II. The mesomer resulting from π donation from the iron(II) atom toward the complexed arene would result in a cumulenic structure (Scheme 8) that would support complexation by the arenophile on the five exterior phenyl carbons. Evidence of the importance of this mesomer for a related compound was given by Matsuzaka et al. (Scheme 9).[23] This group obtained a crystal structure that clearly showed unequal Ru−C bond lengths about a flat benzenoid ring, which was part of a fused-ring polyaromatic metallocycle. Furthermore, the decrease of the C≡C bond stretch induced by the coordination of the (η^5-Cp*)Ru$^+$ fragment onto the phenyl ring is relatively large ($25 < \Delta\nu_{C\equiv C} < 71$ cm^{-1}). These values are larger than those for strongly electron-withdrawing groups such as NO_2, which favor a strong reorganization of the π-electron system from the metal to the heteroatoms. In addition, after oxidation of the iron center the inversion of the polarization of the π-electron system observed for type I complexes does not occur. Indeed, the π-electrons of the aromatic ring engaged in the complexation with the Ru atom are not available to allow a stabilization of the Fe^{III} center, and the charge-delocalized mesomer II (Scheme 8) includes a high-energy vinylic cation. From these data, it cannot be concluded that the Ru terminus is a stronger π acceptor than the nitro group, but the electron-withdrawing character and the impact of its coordination on the aryl ring taken as a whole make the (η^5-Cp*)Ru$^+$ fragment more efficient than the nitro group at weakening the electron density on the (η^2-dppe)(η^5-Cp*)Fe end-group.

(21) Randic, M. *Chem. Rev.* **2003**, *103*, 3449−3606.

(22) Schrader, B. *Infrared and Raman Spectroscopy. Methods and Applications*; VCH: Weinheim, 1995.

Table 3. Bond Lengths (Å) and Angles (deg)

	2[PF$_6$]	**2[PF$_6$]$_2$**[a]	**4**	**4[PF$_6$]**	**6A[PF$_6$]**	**6B[PF$_6$]**	**6B[PF$_6$]$_2$**
			Bond Lengths				
Fe−P1	2.1870(13)	2.256(2) 2.259(3) 2.277(2)	2.1689(6)	2.2911(12)	2.1795(15)	2.1933(9)	2.2787(14)
Fe−P2	2.1779(13)	2.276(3) 2.283(2) 2.271(3)	2.1608(6)	2.2436(11)	2.1783(17)	2.2050(9)	2.3105(14)
Fe−C37	1.889(5)	1.900(8) 1.886(9) 1.884(8)	1.895(2)	1.888(5)	1.890(5)	1.880(3)	1.905(5)
C37−C38	1.230(6)	1.211(10) 1.223(11) 1.214(10)	1.223(3)	1.253(7)	1.216(7)	1.225(4)	1.214(7)
C38−C39	1.424(6)	1.421(11) 1.419(11) 1.425(11)	1.440(3)	1.424(7)	1.433(8)	1.427(4)	1.429(7)
C39−C40	1.433(7)	1.400(12) 1.463(11) 1.438(10)	1.378(3)	1.399(7)	1.422(8)	1.367(4)	1.360(7)
C40−C41	1.405(7)	1.450(12) 1.425(11) 1.436(12)	1.409(4)	1.375(7)	1.424(9)	1.416(4)	1.424(8)
C41−C42	1.419(8)	1.404(13) 1.411(10) 1.366(13)	1.384(4)	1.345(7)	1.399(10)	1.365(5)	1.340(10)
C42−C43	1.393(8)	1.356(13) 1.406(11) 1.415(13)	1.403(4)	1.410(6)	1.408(9)	1.438(5)	1.419(9)
C39−C44[b] or C48[c]	1.433(7)[b]	1.445(11) 1.410(10) 1.423(11)	1.432(3)[c]	1.439(7)[c]	1.445(8)‡	1.438(4)[c]	1.444(7)[c]
C43−C44[b] or C48[c]	1.416(7)	1.429(12) 1.413(11) 1.412(12)	1.427(3)	1.434(6)	1.432(8)	1.447(4)	1.446(7)
C47−C48			1.417(3)	1.404(6)	1.436(9)	1.454(4)	1.430(7)
C46−C47			1.364(4)	1.343(7)	1.351(9)	1.404(4)	1.396(7)
C45−C46			1.403(4)	1.374(8)	1.385(11)	1.408(5)	1.398(8)
C44−C45			1.360(4)	1.365(7)	1.340(11)	1.387(5)	1.399(9)
C43−C44			1.423(4)	1.438(7)	1.438(10)	1.425	1.420(8)
Fe−Cp*$_{centroid}$	1.748	1.790 1.774 1.785	1.737	1.779	1.757	1.746	1.801
Ru−Cp*$_{centroid}$	1.809	1.817 1.813 1.805			1.798	1.797	1.807
Ru−Ar$_{centroid}$	1.655	1.718 1.700 1.712			1.739	1.731	1.731
			Bond Angles				
P1−Fe−P2	85.72(5)	84.55(9) 84.76(9) 85.57(9)	85.37(2)	84.10(4)	85.64(6)	86.60(4)	84.71(5)
P1−Fe−C37	88.69(13)	84.4(2) 81.8(2) 80.6(3))	85.22(7)	99.37(14)	86.63(16)	87.56(8)	91.59(15)
P2−Fe−C37	86.75(14)	94.1(3) 92.5(2) 94.6(3)	82.93(7)	79.50(13)	84.83(15)	81.12(8)	84.03(15)
Fe−C37−C38	172.0(4)	171.6(7) 175.7(7) 169.0(7)	175.4(2)	164.3(4)	177.9(4)	177.4(2)	173.1(5)
C37−C38−C39	172.9(5)	171.2(9) 171.1(9) 176.3(8)	174.4(3)	176.5(5)	166.3(6)	171.8(3)	173.1(6)
C40−C39−C44[b] or 48[c]	117.2(4)[b]	117.2(8) 117.2(8) 118.1(7)	118.6(2)[c]	118.8(4)[c]	116.6(5)[c]	117.6(2)[c]	117.7(5)[c]
C41−C42−C43	119.2(4)	122.3(10) 122.8(8) 120.6(10)	119.2(2)	120.0(5)	120.8(6)	119.7(3)	121.0(6)
C48−C47−C46			119.9(2)	121.8(5)	119.7(6)	120.6(3)	120.8(5)
C43−C44−C45			122.2(3)	121.0(5)	120.6(7)	120.9(3)	121.6(5)
Ar$_{centroid}$−Ru−Cp*$_{centroid}$	177.4	179.0 177.9 178.7			179.1	179.1	178.8
Cp*$_{centroid}$−Fe−C37	118.3	119.7 121.4 120.2	119.7	117.7	121.0	121.3	121.2

[a] There are three molecules and four disordered dichloromethane molecules in the asymmetric unit. [b] Data refer to phenyl bridging carbon, C44. [c] Data refer to naphthyl bridging carbon, C48

Scheme 8. Cumulenic, Charge-Separated Mesomer of (I) 2[PF$_6$] and (II) 2[PF$_6$]$_2$ Resulting from Donor−Acceptor Interactions

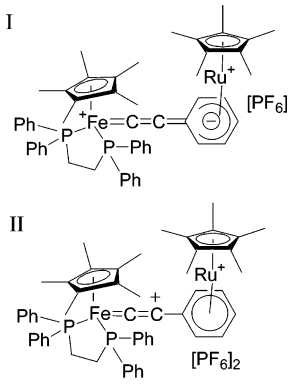

Scheme 9. Inter-ring Haptotropic Rearrangement of (η^5-Cp*)Ru$^+$ Observed by Matsuzaka et al.[23]

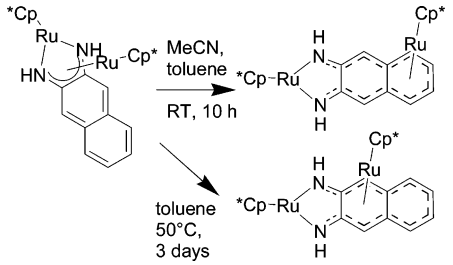

Upon complexation to the arenophile, the iron(II) naphthyl derivative IR stretch also decreases (**4** vs **6B[PF$_6$]**, $\Delta\nu_{C\equiv C}$ = 14 cm^{-1}), a fact that may be attributed to a small increase of the weight of mesomer B in the description of the electronic structure. Upon oxidation, the peaks of both **4[PF$_6$]** and **6B-[PF$_6$]$_2$** are split in two, as commonly occurs for type I compounds.[11a] The frequency of the C≡C stretch of organoiron, **4**, decreases much more (62 < $\Delta\nu_{C\equiv C}$ < 122 cm^{-1}) than that of the binuclear daughter complex, **6B[PF$_6$]** (0 < $\Delta\nu_{C\equiv C}$ < 22 cm^{-1}). This indicates that a cumulenic, quinoidal mesomer (Schemes 1 and 8) plays a larger role in the description of the electronic structure of oxidized organoiron, **4[PF$_6$]**, than for its ruthenium-containing homologue, due to the electronic properties of the (η^5-Cp*)Ru$^+$ arenophile.

X-ray Crystal Structures. Monocrystals of **2[PF$_6$]**, **2[PF$_6$]$_2$**, **4**, **4[PF$_6$]**, **6A[PF$_6$]**, **6B[PF$_6$]**, and **6B[PF$_6$]$_2$** were grown by the slow diffusion of a nonsolvent into a concentrated solution of the product (see Experimental Section). The diffractometric parameters are given in Table 2, and interesting bond lengths and angles are given in Table 3. The resulting structures (excluding hydrogen atoms, counterions, and solvent molecules) are shown in the ORTEP diagrams in Figures 2a−g. The numbering of the phenyl and naphthyl rings is C39−44 and C39−48, respectively, following the exteriors of the rings, starting from the substituted carbon, C39. The salt **2[PF$_6$]$_2$** crystallizes in the monoclinic space group $P2_1/n$, and three nonequivalent molecules were found in the unit cell. As a consequence, the structural parameters are less accurate for this heterobimetallic complex. Since the heterobimetallic naphthyl derivatives **6A[PF$_6$]**, **6B[PF$_6$]**, and **6B[PF$_6$]$_2$** exhibit planar chirality, attention was paid to whether these compounds crystallized into a non-centrosymmetric space group, as such a result may indicate the crystallization of a single enantiomer. Optical polarimetry was conducted on crystals of **6B[PF$_6$]$_2$**, which was the only one to have a non-centrosymmetric space group ($P2_1/c$). Unfortunately, the crystals showed no optical activity, indicating that both enantiomers crystallized in equal proportions within one crystal.

For complex **2[PF$_6$]**, the bond distances between the Ru atom and the carbon atoms of the phenyl ring are very similar. They range from 2.203 to 2.214 Å (average 2.220 Å) with a Ru−C_{ipso} distance being slightly longer (2.270 Å). In the Fe(III) derivative, **2[PF$_6$]$_2$**, the coordination of the Ru atom is very similar (average bond distances 2.216 Å, Ru−C_{ipso} 2.288 Å). The 2−3% lengthening of the Ru−C_{ipso} bond lengths versus Ru−C_{Ar} average lengths is not associated with a deformation of the phenyl ring, which remains planar in both cases, clearly indicating that the (η^5-Cp*)Ru$^+$ entity is firmly η^6-coordinated. This evidence of the π-accepting nature of the arenophile is in agreement with the IR data reported above and the structural data found by Matsuzaka et al. (Scheme 9).[23] The X-ray analysis reveals that the π donation from the electron-rich iron terminus to the electron-withdrawing arenophile is not associated with a partial decoordination of the Ru atom.

It is noteworthy that the complexation of the arenophile, (η^5-Cp*)Ru$^+$, in **2[PF$_6$]** (Figure 2a) engenders some interesting changes in molecular geometry with respect to the reference molecule and precursor, **1**.[11a] Upon complexation, the dppe ligand retreats from the iron atom, while the Cp* ligand undergoes no displacement. The retreat of the dppe ligand suggests reduced Fe back-bonding due to the electron-withdrawing nature of the arenophile. The Fe−C37 bond shortens slightly, by 0.005 Å, a value that is within the error of the measurement, and the C37−C38 triple bond lengthens by 0.020 Å with respect to **1**. This is in agreement with a reduction in C37−C38 bond order as shown by the decrease in IR stretching frequency upon complexation (see above and Table 1). However, the coordination of the arenophile seems to limit the structural reorganization of the alkynyl fragment. The contribution of the mesomer II (Scheme 1) is much smaller in **2[PF$_6$]** than in **1**.

Finally the large degree of steric encumbrance is obvious from the structural data. For example, the angle formed between the Ru ligand centroids and the focal Ru atom (177.4°) slightly deviates from linearity probably due to steric hindrance from the ligated iron terminus. These steric constraints are also nicely illustrated in Figure 2a with the curvature of the Fe···C39 segment (Fe−C37−C38 = 172.0(4)° and C37−C38−C39 = 172.9(5)°).

Oxidation of **2[PF$_6$]** to give **2[PF$_6$]$_2$** (Figure 2b) results in the retreat of all ligands from the iron atom, while the Ru−$C_{aryl-centroid}$ distance increases from 1.655 Å to ca. 1.710 Å. Meanwhile, the average Ru−C_{aryl} distance is almost unchanged and the Cp*Ru unit is weakly displaced away from the iron center, indicating that the steric constraints probably increase upon oxidation of the iron center.

Between the mononuclear iron(II) and iron(III) compounds, **4** and **4[PF$_6$]** (Figure 2), respectively, the molecular geometry is perturbed in such a fashion that is in agreement with previous findings for compounds of type I (Scheme 1).[11a] In brief, the Fe−Cp*$_{centroid}$ and Fe−P bonds are lengthened upon oxidation, whereas the Fe−C37 bond is slightly shortened. Furthermore, the C37≡C38 triple bond length significantly increases (see Table 3). In addition, the marked general lengthening of the C−C aromatic bonds of the naphthalene fragment points toward the importance of the IV mesomer upon oxidation (Scheme 1). Finally, the amplitude of bond length alternation around the naphthyl rings is exaggerated in the case of **4[PF$_6$]** as compared to **4** (Table 3). This fact points to a decrease in aromaticity upon

(23) Takemoto, S.; Oshio, S.; Shiromoto, T.; Matsuzaka, H. *Organometallics* **2005**, *24*, 801−804.

the loss of electron density. This is in accord with the prediction of Hückel's rule requiring a $(2n+2)\pi$ integral electron count for aromatic rings. Finally, one can note that the Fe(II)−C37≡C38 fragment of **4** mildly deviates from linearity (175.4(2)°), as has been reported for other compounds of type I,[11a] and this bending occurs to a greater extent (164.2(4)°) upon oxidation to Fe(III), **4[PF$_6$]**.

A further iron(II)−iron(III) structural contrast can be made between **6B[PF$_6$]** and **6B[PF$_6$]$_2$**. The iron(II) species crystallizes into the rotational conformer in which (η^5-Cp*)Fe and (η^5-Cp*)-Ru$^+$ fragments are cofacial with respect to the naphthyl plane (Figure 2e), while the opposite conformer is chosen for the iron-(III) species (Figure 2f). All iron(III) ligands retreat from the metal with respect to the iron(II) product (see Table 3), whereas the Fe−C37 bond weakly shortens upon oxidation in the case of the mononuclear precursor, **4**. In agreement with the results for **4**/**4[PF$_6$]**, the bending of the Fe−C37≡C38 fragment also increases (by 4°) upon oxidation of **6B[PF$_6$]** to **6B[PF$_6$]$_2$**. Comparison of the variation of the bond distances in the coordination sphere of the iron atom upon oxidation to form complexes **4[PF$_6$]** and **6B[PF$_6$]$_2$** suggests that the presence of the (η^5-Cp*)Ru$^+$ fragment on cycle B does not significantly affect the reorganization of the coordination sphere of iron upon electron transfer. However, one notes that ring **A** geometry is less perturbed by oxidation of the iron center in the case of **6B[PF$_6$]** (av difference in bond length, 0.01067 Å) than in that of **4** (0.04183 Å). In both cases, the average C−C naphthalene bond length decreases upon oxidation.

It is of interest to contrast the molecular geometries of the naphthyl acetylide iron(II) species before (**4**) and after complexation (**6A[PF$_6$]** and **6B[PF$_6$]**). Both **6A[PF$_6$]** (Figure 2g) and **6B[PF$_6$]** (Figure 2e) crystallize as the conformer in which (η^5-Cp*)Fe and (η^5-Cp*)Ru$^+$ are on the same face of the naphthyl plane. For both regioisomers, Fe−Cp* and Fe−P bonds lengthen upon complexation of the arenophile (Table 3). However, the increase of the Fe−P bond distances is much larger in **6B[PF$_6$]** than in **6A[PF$_6$]**, indicating that the arenophile modifies the electronic properties of the iron center more efficiently when it is coordinated on the side cycle (cycle B) of the naphthalene fragment than on the cycle A linked onto the metal alkynyl. This confirms that the coordination of the arenophile on cycle B favors the electronic delocalization and increases the weight of the cumulenic mesomer like mesomer II (Scheme 1), whereas complexation of the (η^5-Cp*)Ru on cycle A has a limited effect (see mesomer II, Scheme 8) due to the reinforcement of the aromaticity of cycle A.

An in-depth analysis of the degree of perturbation of naphthalene aromaticity upon arenophile complexation can be obtained by comparing the naphthyl geometries before and after complexation. In general, for both naphthyl rings of both regioisomers **6A[PF$_6$]** and **6B[PF$_6$]**, bonds within the complexed ring in both cases incorporate less overall bond length deviation and a smaller and less regular amplitude of bond length alternation than for the corresponding ring in **4**.[20] For noncomplexed naphthalene rings in **6A[PF$_6$]** and **6B[PF$_6$]**, the overall deviation in bond length and the amplitude of bond length alternation are greater than for **4**. The reduction in bond length alternation observed for both regioisomers **6A[PF$_6$]** and **6B-[PF$_6$]** for the complexed rings suggests that the π-bonding electrons of such a ring can be described as being more delocalized, more equally shared among the six aromatic carbon bonds. In contrast, the noncomplexed ring in both regioisomers exhibits exaggerated bond alternation. In conclusion, the arenophile complexation reduces the aromaticity of adjacent rings, while complexed rings display increased aromaticity. Such a change in aromaticity largely accounts for the difference in electron transfer and exchange properties within this series.

Table 4. UV−Vis Absorption Data in CH_2Cl_2

compd	absorption γ/nm ($10^3 \leq$/dm^3 mol^{-1} cm^{-1})
1[7a]	277 (sh, 14,5); 350 (6.6)
1[PF$_6$][7c]	261 (sh, 32.6); 280 (sh, 27.4); 301 (sh, 18.8); 342 (sh, 5.9); 379 (sh, 3.6); 575 (sh, 2.3); 662 (3.1)
2[PF$_6$]	161 (sh, 11.3); 402 (9.1)
2[PF$_6$]$_2$	422 (3.9); 515 (3.5)
4	433 (12.8)
4[PF$_6$]	496 (2.9); 772 (2.8)
6B[PF$_6$]	329 (sh, 11.5); 569 (7.9)
6B[PF$_6$]$_2$	354 (6.6); 415 (6.6); 508 (4.2); 791 (1.3)

UV−Visible Spectroscopy. UV−visible spectra for this novel family of ethynyl compounds are compared in Table 4. The data resemble spectra for previously studied type I compounds, for which the principle absorptions above 270 nm were attributed to MLCT (iron(II) and iron(III) complexes) or LMCT (iron(III) complexes) bands.[11] Complexation of the arenophile results in a red shift of the MLCT band observed for iron(II) species. For example, compared to that of their respective precursors **1** and **4**, this band undergoes a large bathochromic shift of 52 nm in the case of **2[PF$_6$]** and of 136 nm for **6B[PF$_6$]**. Such a bathochromic shift indicates a decrease in the HOMO−LUMO gap upon complexation. The reduction in the HOMO−LUMO gap for the latter provides evidence that the metal-centered HOMO electrons are more polarizable when the arenophile resides on the **B** ring. In comparison with type I compounds (Scheme 1), the UV-vis data indicate that the electron-withdrawing effect of the (η^5-Cp*Ru) arenophile falls between those of the nitro and cyano groups.[11c]

Moreover, the LMCT band, the lowest energy absorption observed for the iron(III) species, is even more sensitive to the position of the arenophile (ring **A** or ring **B**). For example, the phenyl ethynyl organoiron(III), **1[PF$_6$]**, absorbs at 662 nm, whereas the dinuclear Fe(III)/Ru(II) complex undergoes the LMCT transition at 515 nm. The large hypsochromic shift of the LMCT band upon **A**-ring complexation amounts to nearly 150 nm for the phenyl series. In other words, the energy of the ligand-centered orbital, HOMO−*n*, should decrease much more upon complexation than does the energy of the HOMO. This suggests that the LMCT transition comes from the aryl-centered orbitals. The large blue shift of this transition provides strong evidence that the phenyl electrons of **2[PF$_6$]** are much less polarizable than those of **1**. Therefore, the arenophile increases hardness of both the iron (HOMO) electrons and aryl (HOMO−*n*) electrons in the phenyl series. On the other hand, the naphthyl iron(III) series is characterized by a small *bathochromic* shift of the LMCT band upon (η^5-Cp*)Ru$^+$ complexation (19 nm). Similarly, this indicates that the aryl electrons are more polarizable after complexation onto the B ring of **4**. These UV-vis spectroscopic data provide further examples, along with IR data, of the opposite effects that **A**-ring and **B**-ring complexation have on the electronic communication across the ethynyl linker.

Cyclic Voltammetry. Table 5 reports the reversible ($i_p^a/i_p^c = 1.0$), one-electron standard redox potentials for the iron(II)−iron(III) couples from the cyclic voltamograms. The reversibility of the oxidation reveals that the iron(III) species are stable at the electrode. Compounds **1**[11a] and **4** exhibit similar peak potentials, with the naphthyl acetylide adduct, **4**, being shifted anodically by 0.014 V, in accordance with a decrease (13 cm^{-1}) of the C−C infrared absorption (see above). The relative facility of oxidation of **4** is attributed to the lower aromaticity of the substituted naphthalene ring, which facilitates

Table 5. Standard Redox Potentials Measured by Cyclic Voltammetry

compd	$E_0(Fe^{II}-Fe^{III})$,[a] V	ref
1	−0.15	7a
2[PF$_6$]	0.090	this work
4	−0.136	this work
6B[PF$_6$]	0.055	this work

[a] Conditions: 0.1 M tetra-*n*-butylammonium hexafluorophosphate in CH_2Cl_2; scan rate = 0.1 V/s, Pt electrodes, V vs SCE (cf. ferrocene/ferrocenium 0.460 V vs SCE).

Table 6. Least-Squares-Fitted Mössbauer Spectroscopic Data

compd	IS[a](QS), mm s^{-1}	Fe^{II} or Fe^{III}	ref
1	0.27 (2.02)	II	14
1[PF$_6$]	0.25 (0.9)	III	14
2[PF$_6$]$_2$	0.21 (0.74)	III	this work
4	0.26 (2.00)	II	this work
4[PF$_6$]	0.28 (0.97)	III	this work
6B[PF$_6$]	0.27 (2.05)	II	this work
6B[PF$_6$]$_2$	0.28 (0.95)	III	this work

iron(III) stabilization through the contribution of mesomer IV (Scheme 1b). Similar aromaticity arguments have been made to describe the electrochemical behavior of related phenyl and anthracenyl acetylide iron compounds.[12a,b]

Complexation of organoirons **1** and **4** by the Cp^*Ru^+ arenophile to give **2[PF$_6$]** and **6B[PF$_6$]**, respectively, results in a large anodic shift in redox potential. Specifically, this difference amounts to 0.240 V for the phenyl adduct (**2[PF$_6$]**) and 0.191 V for the naphthyl one (**6B[PF$_6$]**) (Table 5). The increased difficulty of oxidation of the iron(II) results from three factors. First, the fact that the bimetallic compounds are already cationic in the iron(II) state plays a role. Second, the electron-withdrawing nature of the arenophile perturbs the electronic environment of the electron-rich iron(II) center. Finally, the trapping of the aromatic π-electrons via coordination to the arenophile affects the formation of the cumulenic/quinoidal mesomer (Scheme 8). The latter two factors play a larger role for **2[PF$_6$]** than for **6B[PF$_6$]**, which explains the much larger anodic shift of the former, in agreement with the spectroscopic data.

Mössbauer Spectral Studies. These spectral data are summarized in Table 6. The results point to the high degree of purity of all products, only one doublet being seen in each spectrum.[24] All compounds, excepting **2[PF$_6$]$_2$**, behave like classical type I compounds in both oxidation states.[11a] Surprisingly, **2[PF$_6$]$_2$**, an iron(III) complex, exhibits much lower isomer shift (IS = 0.21 mm/s) and quadrupole splitting (QS = 0.74 mm/s) values. The IS parameter is known to be very sensitive to the electronic density about the iron nucleus. It is possible that the positive charge around the Ru center is sensed by the iron nucleus both through bonding and, considering the small Fe−Ru distance, through space. The QS value for **2[PF$_6$]$_2$** is exceptionally small. It is significantly lower than for the iron(III) type I compound substituted with NO_2. This observation is consistent with a lower Fe−C_α bond order[18L,25] within **2[PF$_6$]$_2$**, in agreement with the IR data (see above). The (η^5-Cp*)Ru^+ arenophile both serves as a strong electron acceptor and effectively prevents the formation of cumulenic mesomer D (Scheme 1).

Electron Spin Resonance Spectroscopy. The spectra for all paramagnetic compounds reported herein were taken both at 77 and, when electronic relaxation proved sufficiently rapid, at 298 K. Table 7 summarizes the results. The spectra of **1[PF$_6$]** and **4[PF$_6$]** nearly appear superimposable at 77 K. However, whereas the complex **1[PF$_6$]** is not ESR active at 298 K, the complex with the naphthyl substituent displays a well-resolved sharp signal allowing the determination of the g_{iso} value at 298 K. Upon warming, the g_{iso} shifts from 2.155 to 2.013. These data taken as a whole suggest that SOMOs are very similar in both complexes, but upon warming reorganization takes place in the case of **4[PF$_6$]** and the ligand character of the radical increases.

Table 7. Electron Spin Resonance Spectroscopic Data

compd	g_1	g_2	g_3	g_{iso}	Δg	g_{iso}[b]	ref
1[PF$_6$]	2.464	2.033	1.975	2.157	0.489		14
2[PF$_6$]$_2$	2.506	2.031	1.972	2.170	0.534		this work
4[PF$_6$]	2.465	2.028	1.973	2.155	0.492	2.013	this work
6B[PF$_6$]$_2$	2.503	2.026	1.971	2.167	0.532	2.010	this work

[a] At 77 K in $CH_2Cl_2/C_2H_4Cl_2$ (1:1) glass unless otherwise noted. [b] At 298 K.

Upon complexation of the (η^5-Cp*)Ru^+ arenophile, the g_1 tensor increases for both the phenyl ethynyl, **2[PF$_6$]$_2$**, and 1-naphthyl acetylide, **6B[PF$_6$]$_2$**, whereas g_2 and g_3 remain almost unchanged. As a consequence, the presence of the arenophile increases both the isotropy (g_{iso}) and anisotropy (Δg) tensors. This is in line with previous observations for Fe(III) type I complexes for which the g_{iso} and Δg values increase with the electron-withdrawing character of the substituents on the phenyl ring.[11c] It has been assumed that ESR anisotropy arises essentially from spin−orbit coupling. The more the unpaired electron is ligand centered, the less anisotropic the ESR signal will be. In addition, its g_{iso} value becomes concomitantly closer and closer to the g_e value (g_e = 2.0023). On the basis of this simple reasoning, we can conclude that the (η^5-Cp*)Ru^+ arenophile increases the iron character of the odd electron, by decreasing the contribution from a cumulenic mesomer of type II (Scheme 8).

Inter-ring Haptotropic Rearrangements. As stated in the Introduction, arene chromium tricarbonyl derivatives have frequently been employed to study inter-ring haptotropic migration focusing on $\eta^6-\eta^6$ metal shifts.[6−8] Such transformations have been observed in sandwich compounds as well. For instance, the (η^5-Cp*)Ru^+ arenophile was shown to undergo inter-ring haptotropic rearrangement in the metallocyclic fused-ring system shown in Scheme 9.[23] Another example, the inter-ring migration of the isolobal dicationic (η^5-Cp*)Ir^{2+} group, was reported in the reaction of [(η^5-Cp*)Ir(O=CMe_2)$_3$][BF_4]$_2$ with 1,2,5,6-tetramethylcorannulene ($C_{20}H_6Me_4$).[26] In both cases, the shifts of the arenophile are likely solvent assisted. In contrast, the absence of residual coordinating solvent to facilitate isomerization may explain the very slow, or nonexistent, migration of the (η^5-Cp*)Ru^+ group generated in situ from [(η^5-Cp*)Ru(μ^3-Cl)]$_4$ and an AgX salt in CD_3NO_2, with $C_{20}H_6Me_4$.[27] In related studies, variable-temperature ^{1}H NMR spectroscopy has ruled out intramolecular migration (ΔG > 20 kcal/mol) of the (η^5-Cp*)Ru^+ unit on the corannulene or acecorannulene surface.[28] On the other hand, Wheeler and co-workers have

(24) (a) Greenwood, N. N. *Mössbauer Spectroscopy*; Chapman and Hall: London, 1971. (b) Varret, F.; Mariot, J.-P.; Hamon, J.-R.; Astruc, D. *Hyperfine Interact.* **1988**, *39*, 67−81.

(25) Guillaume, V.; Thominot, P.; Coat, F.; Mari, A.; Lapinte, C. *J. Organomet. Chem.* **1998**, *565*, 75−80.

(26) Alvarez, C. M.; Angelici, R. J.; Sygula, A.; Sygula, R.; Rabideau, P. W. *Organometallics* **2003**, *22*, 624−626.

(27) Vecchi, P. A.; Alvarez, C. M.; Ellern, A.; Angelici, R. J.; Sygula, A.; Sygula, R.; Rabideau, P. W. *Organometallics* **2005**, *24*, 4543−4552.

(28) (a) Seiders, T. J.; Baldridge, K. K.; O'Connor, J. M.; Siegel, J. S. *J. Am. Chem. Soc.* **1997**, *119*, 4781−4782. (b) Seiders, T. J.; Baldridge, K. K.; O'Connor, J. M.; Siegel, J. S. *Chem. Commun.* **2004**, 950−951.

shown[29] that the regioselectivity of (η^5-Cp*)Ru$^+$ *complexation* onto monosubstituted naphthalenes favors more electron-rich rings and that, in some instances, sterics plays a role even more important than that played by electronics. We found the same to be true for inter-ring haptotropic migration, as detailed below.

Among the reactions described in the present study, two were expected to give rise to chemically and redox induced inter-ring haptotropic rearrangements of the (η^5-Cp*)Ru$^+$ arenophile on the basis of steric and electronic arguments. As previously reported,[8] we expected to see a switch from the **B** haptotropomer to the **A** one (Scheme 3) upon the deprotonation of **5B[PF$_6$]$_2$**. Upon deprotonation, the steric encumbrance of the **A** ring was expected to be reduced to a larger extent than for the **B** ring. Furthermore, the strongly *electron-donating* organoiron substituent loses its positive charge upon deprotonation, and full conjugation is restored along the ethynyl linker. All three of these factors were expected to favor inter-ring slippage of the arenophile onto the substituted naphthyl ring. In agreement with the above arguments, the deprotonation of **5B[PF$_6$]$_2$** yielded some of the **A** haptotropomer, **6A[PF$_6$]**, along with the major product, **6B[PF$_6$]**, in a 1:11 spectroscopic ratio (8 mol % underwent inter-ring haptotropic rearrangement, while 92% did not) in MeOH/THF solution at room temperature.

More interestingly, based on X-ray data, we thought that an oxidation state dependent contraction/elongation of the Fe−C39 segment might work in conjunction with electronics in favor of a redox-initiated inter-ring haptotropic rearrangement of the arenophile. Therefore, a regiopure sample of **6B[PF$_6$]**, which is thermally stable and does not interconvert into **6A[PF$_6$]**, was subjected to chemical oxidation and reduction cycles. The oxidation was carried out as described in the Experimental Section. Upon treatment of the resulting solution with cobaltocene at ambient temperature, the ratio **6A[PF$_6$]**:**6B[PF$_6$]** was determined to be 6:94 by NMR. We were curious to see whether the percentage to undergo inter-ring migration can be cumulative. Therefore, we subjected a regiopure sample of **6B[PF$_6$]** to two successive chemical redox cycles. After the second cycle, about 12% of the product had been converted to regioisomer **A**. The small degree of haptotropic rearrangement induced during the oxidation/reduction cycle was *not* accompanied by decomplexation of the arenophile. The low overall degree of both above-mentioned inter-ring haptotropic rearrangements is accounted for by the steric encumbrance in both haptotropomers in both oxidation states.

Conclusions

In this contribution, we have detailed the efficient syntheses and complete spectroscopic and structural characterizations of a novel family of mono- and heterobinuclear acetylide complexes. These complexes feature an electron-rich (η^2-dppe)(η^5-Cp*)Fe end-group and another end-group of variable aromaticity as well as steric and electronic environment, sometimes including a cationic ruthenium sandwich complex. These syntheses are noteworthy in that they exhibit regioselective complexation of the (η^5-Cp*)Ru$^+$ arenophile onto either a phenyl, **2[PF$_6$]**, or a naphthyl, **5B[PF$_6$]$_2$**, **6A[PF$_6$]**, and **6B[PF$_6$]**, ring in the presence of four free and electron-rich phenyl rings. This preference is explained by both the steric encumbrance of the dppe phenyl rings and the excellent overlap between the electron-rich iron acetylide substituent and the ethynyl phenyl and naphthyl rings. Furthermore, the electron transfer properties among the complexes were roundly revealed to change as a function of whether the arenophile was collinear with the ligated iron (as in **2[PF$_6$]** and **6A[PF$_6$]**) or found on the unsubstituted naphthyl ring (**6B[PF$_6$]**). In addition, this work represents the first thorough study of the changing electronic and steric environments of an arenophile on both the substituted and unsubstituted naphthyl rings between which it moves. The electron-withdrawing character, specifically the trapping of the aromatic π electrons, renders the (η^5-Cp*)Ru$^+$ fragment more efficient than the nitro group at reducing the electron density on the redox-active (η^2-dppe)(η^5-Cp*)Fe end-group.

Finally, a small degree of haptotropic rearrangement of the (η^5-Cp*)Ru$^+$ arenophile was shown to occur at room temperature between the two naphthyl rings upon in situ variation of the electronic and steric environments. The low overall degree of inter-ring haptotropic rearrangement is accounted for by the steric encumbrance in both haptotropomers. A significant decrease in total steric strain might solve the above-mentioned problems and give rise to better yields of inter-ring haptotropic rearrangements upon deprotonation, oxidation, and reduction. In this vein, syntheses incorporating a less bulky arenophile are currently under way.

Experimental Section

General Procedures. Manipulations of air-sensitive compounds were performed under an argon atmosphere using standard Schlenk techniques or in an argon-filled Jacomex 532 drybox. Tetrahydrofuran (THF), diethyl ether, toluene, and pentane were dried and deoxygenated by distillation from sodium/benzophenone ketyl. Acetone was distilled from P_2O_5. Dichloromethane and dichloroethane were distilled under argon from P_2O_5 and then from Na_2CO_3. Methanol was distilled over dried magnesium turnings. The following compounds were prepared following published procedures: 1-ethynylnaphthalene,[30] ferrocenium hexafluorophosphate [Fe(η^5-Cp)$_2$][PF$_6$](FcPF$_6$),[31] (η^2-dppe)(η^5-Cp*)Fe−Cl,[32] (η^2-dppe)(η^5-Cp*)Fe−C≡C−Ph (**1**),[11a] and [(η^5-Cp*)Ru(CH$_3$CN)$_3$][PF$_6$].[13,14] Potassium *tert*-butoxide (ACROS) was used without further purification. Infrared spectra were obtained as Nujol mulls or as films between KBr windows with a Bruker IFS28 FTIR infrared spectrophotometer (4000−400 cm^{-1}). UV−visible spectra were recorded on a UVIKON XL spectrometer. ^{1}H, ^{13}C, and ^{31}P NMR spectra were recorded on a Bruker DPX200, Avance 300, or Avance 500 NMR multinuclear spectrometer at ambient temperature, unless otherwise noted. Chemical shifts are reported in parts per million (δ) relative to tetramethylsilane (TMS), using the residual solvent resonances as internal references. Coupling constants (J) are reported in hertz (Hz), and integrations are reported as numbers of protons. The following abbreviations are used to describe peak patterns: br = broad, s = singlet, d = doublet, dd = double doublet, t = triplet, h = heptet, m = multiplet. ^{1}H and ^{13}C NMR peak assignments are supported by the use of COSY, HMQC, and HMBC experiments. High-resolution mass spectra (HRMS) were recorded on a high-resolution ZabSpec TOF VG analytical spectrometer operating in the ESI$^+$ mode, at the Centre Régional de Mesures Physiques de l'Ouest (CRMPO), Rennes. Poly(ethylene glycol) (PEG) was used as internal reference, and dichloromethane was used as solvent. EPR spectra were recorded on a Bruker EMX-8/2.7 (X-band) spectrometer. The ^{57}Fe Mössbauer spectra were recorded with a 2.5 × 10^{-2} C (9.25 × 10^8 Bq) ^{57}Co source using a symmetric triangular sweep mode. Computer fitting of the Mössbauer data to Lorentzian line shapes was carried out with a

(29) Wheeler, D. E.; Hill, S. T.; Carey, J. M. *Inorg. Chim. Acta* **1996**, *249*, 157−161.

(30) John, J. A.; Tour, J. M. *Tetrahedron* **1997**, *53*, 15515−15534.

(31) Connelly, N. G.; Geiger, W. E. *Chem. Rev.* **1996**, *96*, 877−910.

(32) Roger, C.; Hamon, P.; Toupet, L.; Rabaa, H.; Saillard, J.-Y.; Hamon, J.-R.; Lapinte, C. *Organometallics* **1991**, *10*, 1045−1054.

previously reported computer program.[33] The isomer shift values are reported relative to iron foil at 298 K. Elemental analyses were conducted on a Thermo-Finnigan Flash EA 1112 CHNS/O analyzer by the Microanalytical Service of the CRMPO at the University of Rennes 1, France, and by Ilse Beetz Microanalytisches Laboratorium, Kronach, Germany.

[(η^2-dppe)(η^5-Cp*)Fe−C≡C−{(η^6-phenyl)Ru(η^5-Cp*)}][PF_6] (2[PF_6]). The previously described product, **1** (0.260 g, 0.377 mmol), and [(η^5-Cp*)Ru($CH_3CN)_3$][PF_6] (0.1715 g, 0.377 mmol, 1 equiv) were combined with 10 mL of CH_2Cl_2. This red solution was stirred overnight at RT, protected from light, and then filtered into a new Schlenk flask. The filtrate was partially precipitated with diethyl ether. The product isolated by filtration was washed twice with 2 mL portions of diethyl ether and dried in vacuo to yield 0.270 g (0.252 mmol) of red powder (69% yield), which was crystallized by slow diffusion of diethyl ether into a concentrated dichloromethane solution of the product. HRMS ESI$^+$: *m*/*z* calcd for $C_{54}H_{59}{}^{56}FeP_2{}^{102}Ru$ (C^+), 927.24849; found, 927.2504. ^{1}H NMR (200 MHz, $CDCl_3$): δ 7.68 (m, 4H, *o*-*Ar* dppe); 7.43 (m, 8H, 4*m*-*Ar* dppe and 4*p*-*Ar* dppe); 7.32 (t, $^3J_{H-H}$ = 6.8 Hz, 4H, *m*-*Ar* dppe); 7.21 (t, $^3J_{H-H}$ = 7.6 Hz, 4H, *o*-*Ar* dppe); 5.53 (t, $^3J_{H-H}$ = 5.6 Hz, 2H, *m*-C_6H_5); 5.45 (d, $^3J_{H-H}$ = 5.2 Hz, 1H, *p*-C_6H_5); 5.06 (d, $^3J_{H-H}$ = 5.8 Hz, 2H, *o*-C_6H_5); 2.46 (m, 2H, CH_2/dppe); 2.02 (m, 2H, CH_2/dppe); 1.75 (s, 15H, Ru−Cp*); 1.34 (s, 15H, Fe−Cp*). ^{13}C{^{1}H} NMR (50 MHz, acetone-d_6): δ 137.15 (br s, C_α); 133.91 (s, *o*-*Ar*/dppe); 133.60 (s, *o*-*Ar*/dppe); 129.64 and 129.53 (s, p-*Ar*/dppe); 127.65 (s, *m*-Ar/dppe); 95.01 (s, Ru-*Cp**); 93.10 (s, *o*-C_6H_5); 88.80 (br s, Fe-*Cp**); 86.27 (s, *m*-C_6H_5); 84.17 (s, *p*-C_6H_5); 84.1 (s, *ipso*-C_6H_5); 29.85 (m, CH_2/dppe); 10.37 (s, Ru−Cp*); 10.22 (s, Fe−Cp*). ^{31}P NMR (81 MHz, acetone-d_6): δ 98.85 (s, dppe); −143.0 (h, $^1J_{P-F}$ = 708 Hz, PF_6).

[(η^2-dppe)(η^5-Cp*)Fe−C≡C−{(η^6-phenyl)Ru(η^5-Cp*)}][PF_6]$_2$ (2[PF_6]$_2$). A 180 mg (0.168 mol) quantity of the Fe(II) complex **2**[PF_6] and 1 equiv (0.056 g, 0.168 mmol) of $FcPF_6$ were combined and cooled to −60 °C under inert atmosphere before being dissolved in cold THF (−60 °C) and allowed to warm to room temperature overnight with stirring. The following morning, a reddish solid was visible in the solution. Enough dichloromethane (30 °C) was added to dissolve the solid, and the product was precipitated from cold diethyl ether. Removal by cannula filter of the supernatant, one diethyl ether washing, and repetition of the partial precipitation yielded 0.175 g (86%) of dark product upon vacuum-drying. Orange, platelike crystals were obtained upon the slow diffusion of pentane into a concentrated dichloromethane solution of product at −20 °C. HRMS (ESI$^+$): *m*/*z* calcd for $C_{54}H_{59}{}^{56}FeP_2{}^{102}Ru$ (C^{2+}), 463.6242; found, 463.6253. ^{1}H NMR (200 MHz, acetone-d_6): δ 15.5 (br s, 2H, Ar*H*); 7.9 (br s, 3H, Ar*H*); 7.6 (br s, 6H, Ar*H*); 6.1 (br s, 3H, Ar*H*); 3.5 (br s, 5H, Ar*H*); 2.8 (s, 3H, Ar*H*); 2.75 (m, 2H CH_2/dppe); 2.7 (s, 15H, Ru−Cp*); 0.8 (m, 2H, C*H*$_2$/dppe); −3.9 (br s, 1H, Ar*H*); −9.7 (br s, 2H, Ar*H*); −11.7 (br s, 15H, Fe−Cp*).

[(η^2-dppe)(η^5-Cp*)Fe=C=CH−1-Naphthyl][BPh_4] (3[BPh_4]). To an excess of freshly made 1-naphthyl acetylene (0.304 g, 2.0 mmol) was added 0.704 g (1.13 mmol) of (η^2-dppe)(η^5-Cp*)FeCl along with 10 mL of MeOH and 3 mL of THF under inert atmosphere. The mixture was stirred at room temperature for 30 min, at which point, 0.386 g (1.13 mmol) of $NaBPh_4$ in THF was added via cannula, and the reaction was stirred overnight at room temperature in the absence of light. The solvents were then evaporated and the solid was extracted with CH_2Cl_2 and partially precipitated from pentane. After one pentane washing (10 mL), the brown, gluey paste was dried under vacuum to yield 1.002 g of brown powder (1.057 mmol, 94%). HRMS (ESI$^+$): *m*/*z* calcd for $C_{48}H_{47}P_2{}^{56}Fe$ (C^+), 741.2502; found, 741.2502. FT-IR (Nujol, cm^{-1}): 1623, 1606 (d, C=C). ^{1}H NMR (200 MHz, $CDCl_3$): δ 7.88−6.56 (m, 47H, *Ar*/dppe, *Ar*/BPh_4, and *Ar*/napht); 5.76 (t, $^4J_{H-P}$ = 4.0 Hz, 1H, H_{vin}); 2.90 (m, 2H, CH_2/dppe); 2.32 (m, 2H, CH_2/dppe); 1.57 (s, 15H, Fe−Cp*). ^{13}C{^{1}H} NMR (75.5 MHz, $CDCl_3$): δ 356.70 (t, $^2J_{P-C}$ = 33 Hz, C_α); 137.0−122.5 (m, Ar/BPh_4, *Ar*/napht, and Ar/dppe); 122.0 (s, C_β); 100.60 (s, Fe-*Cp**); 30.15 (m, CH_2/dppe); 10.78 (s, Fe−Cp*). ^{31}P NMR (81 MHz, $CDCl_3$): δ 88.74 (s, dppe). Anal. Calcd for $C_{72}H_{67}BP_2Fe$: C, 81.51; H, 6.37. Found: C, 81.65; H, 6.53.

[(η^2-dppe)(η^5-Cp*)Fe=C=CH−1-Naphthyl][PF_6] (3[PF_6]). An excess of freshly deprotected 1-naphthyl acetylene (1.09 equiv, 0.250 g, 1.64 mmol) was combined with $NaPF_6$ (1.2 equiv, 0.3023 g, 1.800 mmol) and stirred in MeOH (20 mL) for 30 min before a THF solution of (η^2-dppe)(η^5-Cp*)FeCl (0.921 g, 1.47 mmol) was added via cannula. The reaction was stirred overnight at room temperature in the absence of light. The solvents were then evaporated and the solid was extracted with CH_2Cl_2 and partially precipitated from pentane to yield a brown, gluey paste. After one pentane washing (10 mL) and vacuum-drying, a brown powder was obtained at a yield of 1.303 g (1.214 mmol, 83%). HRMS (ESI$^+$): *m*/*z* calcd for $C_{48}H_{47}P_2{}^{56}Fe$ (C^+), 741.25024; found, 741.2482. FT-IR (Nujol, cm^{-1}): 1588 and 1510 s. ^{1}H NMR (200 MHz, acetone-d_6): δ 7.94−6.73 (m, 27H, *Ar*/dppe, *Ar*/napht); 5.79 (t, $^4J_{H-P}$ = 4.4 Hz, 1H, H_{vin}); 3.29 (m, 2H, CH_2/dppe); 2.77 (m, 2H, CH_2/dppe); 1.74 (s, 15H, Fe−Cp*). ^{31}P NMR (81 MHz, acetone-d_6): δ 88.95 (s, dppe); −143.0 (h, $^1J_{P-F}$ = 708 Hz, PF_6).

[(η^2-dppe)(η^5-Cp*)Fe−C≡C−1-Naphthyl] (4). To 1.002 g (1.057 mmol) of **3**[BPh_4]) was added 1.2 equiv of *t*-BuOK (142 mg) along with 10 mL of MeOH and 5 mL of THF. The mixture was stirred at room temperature for 2 h, after which the solvents were evaporated under vacuum, and the remaining solid was extracted in THF and partially precipitated from methanol. The resulting precipitate was washed three times with pentane and vacuum-dried to yield 0.630 g of orange powder (0.85 mmol, 81%), from which crystals were obtained via the slow diffusion of methanol into a concentrated dichloromethane solution of the product. HRMS (ESI$^+$): *m*/*z* calcd for $C_{48}H_{46}P_2{}^{56}Fe$ (C^+), 740.2424; found, 740.2419. ^{1}H NMR ($CDCl_3$, 200 MHz): δ 8.09 (t, 4H, $^3J_{H-H}$ = 7.8 Hz, H*Ar*/dppe); 8.02 (d, 1H, $^3J_{H-H}$ = 9.6 Hz, H*Ar*); 7.86 (d, 1H, $^3J_{H-H}$ = 8.0 Hz); 7.6−7.3 (m, 19H, H*Ar*); 7.20 (t, 1H, $^3J_{H-H}$ = 7.2 Hz, H*Ar*); 7.1 (d, 1H, $^3J_{H-H}$ = 7.2 Hz, H*Ar*); 2.77 (m, 2H, dppe) 2.05 (m, 2H, dppe); 1.54 (s, 15H, FeCp*). ^{13}C{^{1}H} NMR ($CDCl_3$, 50.3 MHz): δ 145.07 (t, $^2J_{P-C}$ = 39.2 Hz, Fe*C*≡C); 139.8−122.1 (m, *Ar*/napt and Ar/dppe); 119.7 (s, FeC≡*C*); 87.83 (s, Fe*Cp**); 30.79 (m, CH_2/dppe); 10.28 (s, FeCp*). ^{31}P NMR ($CDCl_3$, 81 MHz): δ 101 (s, dppe). Anal. Calcd for $C_{48}H_{46}FeP_2{\cdot}CH_3OH$ (crystallization solvent): C, 76.16; H, 6.52. Found: C, 75.80; H, 6.28.

[(η^2-dppe)(η^5-Cp*)Fe−C≡C−1-Naphthyl][PF_6] (4[PF_6]). The Fe(II) complex, **4** (0.260 g, 0.232 mmol), and 0.92 equiv (0.073 g, 0.213 mmol) of $FcPF_6$ were combined and cooled to −60 °C under inert atmosphere before being dissolved in cold THF (−60 °C) and allowed to warm to room temperature overnight with stirring. The following morning, the solution was concentrated and the product precipitated from a 4:1 mixture of cold ether/pentane. Removal by cannula filter of the supernatant and vacuum-drying yielded 0.206 g (70%) of a very dark powder, which formed orange, platelike crystals by slow diffusion of pentane into a concentrated dichloromethane solution of the product. HRMS (ESI$^+$): *m*/*z* calcd for $C_{48}H_{46}{}^{56}FeP_2$ (C^+), 740.2424; found, 740.2415. ^{1}H NMR (300 MHz, acetone-d_6): δ 33.06 (s, 1H, Ar*H*); 16.74 (br s, 1H, Ar*H*); 16.37 (s, 1H, Ar*H*); 6.94 (s, 4H, Ar*H*); 6.67 (s, 1H, Ar*H*); 6.50 (s, 1H, Ar*H*); 3.82 (s, 5H) 2.08 (br s, 2H, CH_2/dppe); −2.60 (s, 1H, Ar*H*); −2.91 (br s, 2H, C*H*$_2$/dppe); −4.91 (s, 1H, Ar*H*); −10.46 (br s, 15H, Fe−Cp*); −52.68 (br s, 1H, Ar*H*); −63.78 (br s, 1H, Ar*H*). ^{31}P NMR (δ,121.5 MHz, acetone-d_6): δ 315 (br s, $w_{1/2}$ = 21200

(33) (a) Boinnard, D.; Bousseksou, A.; Dworkin, A.; Savariault, J.-M.; Varret, F.; Tuchagues, J.-P. *Inorg. Chem.* **1994**, *33*, 271−281. (b) Varret, F. *International Conference on Mössbauer Effects Applications*; Jaipur, India, 1981; Varret, F., Ed.; Indian Science Academy: New Delhi, 1982.

Hz, dppe); −143.6 (h, $^1J_{P-F}$ = 708 Hz, PF_6). Anal. Calcd for $C_{48}H_{46}F_6FeP_3$: C, 65.10; H, 5.24. Found: C, 65.21; H, 5.58.

[(η^2-dppe)(η^5-Cp*)Fe═C═CH−1-{(η^6-naphthyl)Ru(η^5-Cp*)}][PF_6]$_2$ (5B[PF_6]$_2$). The iron vinylidene, **3[PF_6]** (1.072 g, 1.21 mmol), and [(η^5-Cp*)Ru(CH_3CN)$_3$][PF_6] (0.5456 g, 0.9 equiv) were cooled to 0 °C under inert atmosphere and combined with 30 mL of CH_2Cl_2. This reddish-orange solution was stirred for 1 h at 0 °C, after which all insoluble ruthenium starting material had been consumed. This solution was then filtered via cannula under argon, and the filtrate was concentrated and partially precipitated with diethyl ether. The brown, gluey paste isolated by filtration was washed multiple times with a mixture of mostly THF and a few drops of dichloromethane until the filtrate was colorless. The product was then dried in vacuo to yield 1.020 g of yellow powder (0.804 mmol, 74% yield), which crystallized into long, yellow fibers by slow diffusion of pentane into a solution of the product in dichloromethane. While the major, isolated, product contained only the **B** regioisomer, the THF washings rinsed away vinylidene starting material as well as a small quantity of the **B** regioisomer and *all* of the present **A** regioisomer. HRMS (ESI$^+$): *m*/*z* calcd for $C_{58}H_{62}P_2{}^{56}Fe^{102}Ru$ (C^{2+}), 489.1360; found, 489.1368. ^{1}H NMR (200 MHz, acetone-d_6): δ 7.83−7.63 (m, 12H, Ar*H*); 7.49−7.21 (m, 10H, Ar*H*); 7.35 (d, napht H-2); 7.20 (t, napht H-3) {the two above peaks are attributable by the use of COSY, HMBC, and HMQC experiments; the determinations of *J*, integration, and precise δ are rendered impossible by the dominance of dppe Ar peaks in the region}; 6.85 (d, $^3J_{H-H}$ = 7.0 Hz, 1H, Napht H-2); 6.72 (d, $^3J_{H-H}$ = 6.0 Hz, 1H, napht H-5); 6.28 (t, $^3J_{H-H}$ = 5.8 Hz, 1H, napht H-6); 6.16 (t, $^3J_{H-H}$ = 5.6 Hz, 1H, napht H-7); 6.01 (d, $^3J_{H-H}$ = 6.2 Hz, 1H, napht H-8); 5.14 (t, $^4J_{H-P}$ = 4.6, 1H, H_{vin}); 3.30 (m, 2H, CH_2/dppe); 2.73 (m, 2H, CH_2/dppe); 1.77 (br s, 15H, Fe−Cp*); 1.70 (s, 15H, Ru−Cp*). ^{13}C{^{1}H} NMR (75.5 MHz, acetone-d_6): δ 353.4 (t, $^2J_{P-C}$ = 34 Hz, C_α); 134.0−125.0 (m, C_{Ar}); 130.8 (s, Napht C-2); 126.1 (s, Napht C-1); 125.2 (s, Napht C-3); 119.5 (s, C_β); 101.3 (s, Fe-*Cp**); 97.80 (s, Napht C-9); 93.9 (s, Napht C-10); 93.93 (s, Ru-*Cp**); 93.46 (s, Napht C-4); 88.47 (s, Napht C-6); 88.23 (s, Napht C-7); 85.57 (s, Napht C-5); 81.82 (s, Napht C-8); 29.85 (m, CH_2/dppe); 9.82 (s, Fe−Cp*); 8.95 (s, Ru−Cp*). ^{31}P NMR (81 MHz, acetone-d_6): δ 86.42 (dd, $^2J_{P-P}$ = 91 Hz, dppe); −143.0 (h, $^1J_{P-F}$ = 707 Hz, PF_6). Anal. Calcd for $C_{58}H_{62}F_{12}P_4FeRu{\cdot}CH_2Cl_2$ (crystallization solvent): C, 52.38; H, 4.77. Found: C, 52.75; H, 4.83.

[(η^2-dppe)(η^5-Cp*)Fe−C≡C−1-{(η^6-naphthyl)Ru(η^5-Cp*)}][PF_6] (6A[PF_6]). Compound **4** (0.300 g, 0.405 mmol) and [(η^5-Cp*)Ru(CH_3CN)$_3$][PF_6] (0.203 g, 0.405 mmol) were combined with 10 mL of CH_2Cl_2 in a Schlenk flask. This red solution was stirred for a minimum of 4 h at RT, protected from light. The solution was then filtered into another Schlenk flask, and the filtrate was partially precipitated with a diethyl ether/pentane solution (4:1). The product isolated by filtration was washed twice with 2 mL portions of diethyl ether and dried in vacuo to yield 0.318 g (0.284 mmol, 70% yield) of deep red powder. This procedure results in a mixture of regioisomers **6A[PF_6]** and **6B[PF_6]** in the ratio a:b = 47:53 (^{1}H NMR), from which platelike, orange crystals of **6A[PF_6]** were formed by slow diffusion of pentane into a THF solution of the mixture. HRMS (ESI$^+$): calcd for $C_{58}H_{61}{}^{56}FeP_2{}^{102}Ru$ (C^+), 977.26414; found, 977.2662. ^{1}H NMR (300 MHz, acetone-d_6, 193 K): δ 8.05 (t, $^3J_{H-H}$ = 7.9 Hz, 2H, Ar*H*); 7.80 (t, $^3J_{H-H}$ = 6.9 Hz, 2H, Ar*H*); 7.70−7.45 (m, 13H, Ar*H*); 7.35 (t, $^3J_{H-H}$ = 6.8 Hz, 2H, Ar*H*); 7.16 (t, $^3J_{H-H}$ = 7.4 Hz, 1H, Ar*H*); 7.08 (t, $^3J_{H-H}$ = 6.9 Hz, 2H, Ar*H*); 6.70 (d, $^3J_{H-H}$ = 8.8 Hz, 1H, Ar*H*); 6.54 (d, $^3J_{H-H}$ = 5.9 Hz, 1H, Napht H-4); 6.08 (t, $^3J_{H-H}$ = 5.4 Hz, 1H, Napht H-3); 5.58 (d, $^3J_{H-H}$ = 5.8 Hz, 1H, Napht H-2); 2.28 (m, 2H, CH_2/dppe); 1.86 (m, 2H, CH_2/dppe); 1.58 (s, 15H, Ru−Cp*); 1.48 (br s, 15H, Fe−Cp*). ^{13}C{^{1}H} NMR (75.5 MHz, $CDCl_3$): δ 135.3−127.0 (m, Ar*C*); 97.64 (s, Napht C-9); 96.87 (s, Napht C-10); 93.53 (s, Napht C-1); 91.7 (s, Ru−*Cp**); 90.9 (s, Napht C-2); 88.6 (br s, Fe−*Cp**); 87.4 (s, Napht C-3); 82.4 (s, Napht C-4); 30.0 (m, CH_2/dppe); 9.94 (s, Fe−Cp*); 8.71 (s, Ru−Cp*). ^{31}P NMR (121.5 MHz, acetone-d_6, 193 K): δ 97.77 (dd, $^2J_{P-P}$ = 16.3 Hz, dppe); −143.0 (h, $^2J_{P-F}$ = 708 Hz, PF_6). Anal. Calcd for $C_{58}H_{61}F_6FeP_3Ru$: C, 62.09; H, 5.48. Found: C, 61.49; H, 5.67.

[(η^2-dppe)(η^5-Cp*)Fe−C≡C−1-{(η^6-naphthyl)Ru(η^5-Cp*)}][PF_6] (6B[PF_6]). A 0.700 g (0.552 mmol) quantity of **5B[PF_6]$_2$** was combined with 0.0804 g (1.3 equiv) of potassium *tert*-butoxide and dissolved in methanol. The solution underwent an immediate color change to purple. After 2 h, the solvent was evaporated and the product extracted with dichloromethane. This solution was concentrated, and the product was precipitated from pentane and dried under vacuum, yielding 0.550 g (0.446 mmol, 80%) of a very dark powder. HRMS (ESI+): calcd for $C_{58}H_{61}{}^{56}FeP_2{}^{102}Ru$ (C^+), 977.26414; found, 977.2667. ^{1}H NMR (200 MHz, acetone-d_6): δ 8.0−7.0 (m, 23H, Ar*H*); 6.55 (d, $^3J_{H-H}$ = 5.6 Hz, 1H, Napht H-5); 6.27 (d, $^3J_{H-H}$ = 6.2 Hz, 1H, Napht H-8); 5.82 (t, $^3J_{H-H}$ = 6.0 Hz, 1H, Napht H-6); 6.08 (t, $^3J_{H-H}$ = 5.6 Hz, 1H, Napht H-7); 2.69 (m, 2H, CH_2/dppe); 2.65 (m, 2H, CH_2/dppe); 1.69 (s, 15H, Ru−Cp*); 1.51 (br s, 15H, Fe−Cp*). ^{13}C{^{1}H} NMR (δ,75.5 MHz, $CDCl_3$): δ 135.3−127.0 (m, Ar); 96.21 (s, Napht C-10); 93.1 (s, Ru−*Cp**); 89.5 (s, Fe−*Cp**); 87.77 (s, napht C-7); 87.65 (s, napht C-6); 85.40 (s, napht C-5); 84.75 (s, napht C-8); 30.0 (m, CH_2/dppe); 9.71 (br s, Fe−Cp*); 8.99 (br s, Ru−Cp*). ^{31}P NMR (121 MHz, acetone-d_6): δ 98.90 (dd, $^2J_{P-P}$ = 412.5 Hz, dppe); −143.0 (h, $^1J_{P-F}$ = 708 Hz, PF_6). Anal. Calcd for $C_{58}H_{61}F_6FeP_3Ru{\cdot}CH_2Cl_2$ (solvate observed in crystal structure): C, 58.72; H, 5.26. Found: C, 58.80; H, 5.47.

[(η^2-dppe)(η^5-Cp*)Fe−C≡C−1-{(η^6-naphthyl)Ru(η^5-Cp*)}][PF_6]$_2$ (6B[PF_6]$_2$). A 0.420 g (0.375 mmol) quantity of the Fe(II) complex, **6B[PF_6]**, and 0.94 equiv (0.1202 g, 0.352 mmol) of $FcPF_6$ were combined and cooled to −60 °C before being dissolved in cold THF (−60 °C) and allowed to warm to room temperature overnight with stirring. The following morning, a solid was visible in the brown solution. Dichloromethane was added to dissolve the solid, and the product was precipitated twice from cold diethyl ether. The brown, gluey paste obtained was washed with diethyl ether and then with THF until the filtrate was colorless, yielding 0.350 g (78%) of pure product upon vacuum-drying. Crystals were obtained via the slow diffusion of diethyl ether into a dichloromethane solution of the product at −4 °C. HRMS (ESI$^+$): calcd for $C_{58}H_{61}F_6{}^{56}FeP_3{}^{102}Ru$ [($C^{2+}PF_6^-$)$^+$], 1122.2302; found, 1122.2306. ^{1}H NMR (300 MHz, acetone-d_6): δ 29.78 (s, 1H, Ar*H*); 13.94 (br s, 1H, Ar*H*); 8.46 (s, 1H, Ar*H*); 7.77 (s, 2H, Ar*H*); 7.58 (s, 1H, Ar*H*); 7.44 (s, 1H, Ar*H*); 6.98 (s, 2H, Ar*H*); 6.38 (s, 1H, Ar*H*); 5.94 (s, 1H, Ar*H*); 4.78 (s, 1H, Ar*H*); 3.61 (s, 2H, Ar*H*); 3.51 (s, 2H, C*H*$_2$/dppe); 2.91 (s, 3H, Ar*H*); 2.64 (s, 1H, Ar*H*); 2.39 (s, 1H, Ar*H*); 2.05 (s, 15H, Ru−Cp*); 1.34 (s, 1H, Ar*H*); 1.30 (s, 1H, Ar*H*); 0.47 (br s, 2H, C*H*$_2$/dppe); −0.26 (br s, 2H, Ar*H*); −6.37 (s, 1H, Ar*H*); −11.34 (s, 15H, Fe−Cp*); −14.06 (br s, 1H, Ar*H*); −40.03 (br s, 1H, Ar*H*); −57.78 (br s, 1H, Ar*H*). ^{31}P NMR (121 MHz, acetone-d_6): δ 340 (br s, $w_{1/2}$ = 21258 Hz, dppe); −143.8 (h, $^1J_{P-F}$ = 708 Hz, PF_6). Anal. Calcd for $C_{58}H_{61}F_{12}FeP_4Ru.CH_3OH$ (crystallization solvent): C, 54.55; H, 5.04. Found: C, 54.15; H, 5.13.

X-ray Crystal Structure Determinations. Single crystals suitable for X-ray crystallography of compounds **2[PF_6]**, **2[PF_6]$_2$**, **4**, **4[PF_6]**, **6A[PF_6]**, **6B[PF_6]**, and **6B[PF_6]$_2$** were obtained as described above and were mounted with epoxy cement on the tip of a glass fiber. Crystal, data collection, and refinement parameters are given in Table 2. All the compounds were studied on a Kappa-CCD Enraf-Nonius FR590 diffractometer equipped with a bidimensional CCD detector employing graphite-monochromated Mo Kα radiation (λ = 0.71073 Å). The cell parameters were obtained with Denzo and Scalepack with 10 frames (psi rotation: 1° per frame).[34] The data collection provided reflections for the seven compounds (Table 2).[35] Subsequent data reduction with Denzo and Scalepack[34] gave the independent reflections (Table 2). The space groups were chosen

based on the systematic absences in the diffraction data. In the crystal lattice of **2[PF_6]$_2$**, four molecules of dichloromethane per asymmetric unit were present in a severely disordered form. They were treated as a diffuse contribution using the program SQUEEZE. All structures were solved with SIR-97, which revealed the non-hydrogen atoms.[36] After anisotropic refinement, the remaining atoms were found in Fourier difference maps. The complete structures were then refined with SHELXL97 by the full-matrix least-squares procedures on reflection intensities (F^2).[37] The absorption was not corrected. In all cases the non-hydrogen atoms were refined with anisotropic displacement coefficients, and all hydrogen atoms were treated as idealized contributions. Atomic scattering factors were taken from the literature.[38] ORTEP views of the compounds were generated with ORTEP-3 for Windows.[39]

Acknowledgment. The authors would like extend hearty thanks to Dr. B. Demerseman (Rennes) for a generous gift of [(η^5-Cp*)Ru(CH_3CN)$_3$][PF_6]. Dr. F. Paul is gratefuly acknowledged for stimulating discussions. Prof. M. Tilset (Oslo, Norway) is acknowledged for his help in acquiring elemental analyses. Thanks are also expressed to J.-Y. Thépot and F. Justaud (Rennes), A. Mari (Toulouse), and Drs. P. Jehan and P. Guénot (CRMPO, Rennes) for skillful assistance in recording ESR, Mössbauer, and high-resolution mass spectra, respectively. The Ministère de l'Education Nationale de l'Enseignement Supérieur et de la Recherche (MENESR, grant for J.S.-T.) is gratefully acknowledged.

Supporting Information Available: Crystallographic files in CIF format for the seven reported X-ray crystal structures are available free of charge via the Internet at http://pubs.acs.org.

OM060575Q

(34) Otwinowski, Z.; Minor, W. Processing of X-ray Diffraction Data Collected in Oscillation Mode. In *Methods in Enzymology*, Macromolecular Crystallography, Part A; Carter, C. W., Sweet, R. M., Eds.; Academic Press: London, 1997; Vol. 276, p 307.

(35) Nonius. *KappaCCD Software*; Nonius B. V.: Delft, The Netherlands, 1999.

(36) (a) Altomare, M. C.; Burla, M.; Camalli, G.; Cascarano, C.; Giacovazzo, A.; Guagliardi, A. G. G.; Moliterni, G.; Polidori, R.; Spagna, R. Sir97: a new tool for crystal structure determination and refinement. *J. Appl. Crystallogr.* **1998**, *31*, 74−77. (b) Van der Sluis, P.; Spek, A. L. *Acta Crystallogr.* **1990**, *A46*, 194−201. (c) Spek, A. L. J. *Appl. Crystallogr.* **2003**, *36*, 7.

(37) Sheldrick, G. M. *SHELX97. Program for the Refinement of Crystal Structures*; University of Göttingen: Göttingen, Germany, 1997.

(38) *International Tables for X-ray Crystallography*; Wilson, A. J. C., Ed.; Kluwer Academic Publishers: Dordrecht, The Netherlands, 1992; Vol. C.

(39) Farrugia, L. J. *J. Appl. Crystallogr.* **1997**, *30*, 565.